Received: 17 April 2021 | Revised: 10 January 2022 | Accepted: 27 January 2022

DOI: 10.1002/jmor.21457

RESEARCH ARTICLE

morphology WILEY

Cranial osteology of *Hypoptophis* (Aparallactinae: Atractaspididae: Caenophidia), with a discussion on the evolution of its fossorial adaptations

Sunandan Das[1] | **Jonathan Brecko**[2,3] | **Olivier S. G. Pauwels**[2] | **Juha Merilä**[1,4]

[1]Ecological Genetics Research Unit, Organismal and Evolutionary Biology Research Programme, Faculty of Biological and Environmental Sciences, FI-00014 University of Helsinki, Helsinki, Finland

[2]Department of Recent Vertebrates, Royal Belgian Institute of Natural Sciences (RBINS), Brussels, Belgium

[3]Royal Museum for Central Africa, Tervuren, Belgium

[4]Division of Ecology and Biodiversity, Faculty of Science, The University of Hong Kong, Pok Fu Lam, Hong Kong SAR

Correspondence
Sunandan Das, Ecological Genetics Research Unit, Organismal and Evolutionary Biology Research Programme, Faculty of Biological and Environmental Sciences, University of Helsinki, Finland.
Email: sdassnake@gmail.com; sunandan.das@helsinki.fi

Funding information
EDUFI fellowship; University of Helsinki LUOVA scholarship

Abstract

Fossoriality evolved early in snakes, and has left its signature on the cranial morphology of many extinct Mesozoic and early Caenozoic forms. Knowledge of the cranial osteology of extant snakes is indispensable for associating the crania of extinct lineages with a particular mode of life; this applies to fossorial taxa as well. In the present work, we provide a detailed description of the cranium of *Hypoptophis wilsonii*, a member of the subfamily Aparallactinae, using micro-computed tomography (CT). This is also the first thorough micro-CT-based description of any snake assigned to this African subfamily of predominantly mildly venomous, fossorial, and elusive snakes. The cranium of *Hypoptophis* is adapted for a fossorial lifestyle, with increased consolidation of skull bones. Aparallactines show a tendency toward reduction of maxillary length by bringing the rear fangs forward. This development attains its pinnacle in the sister subfamily Atractaspidinae, in which the rear fang has become the "front fang" by a loss of the part of the maxilla lying ahead of the fang. These dentitional changes likely reflect adaptation to subdue prey in snug burrows. An endocast of the inner ear of *Hypoptophis* shows that this genus has the inner ear typical of fossorial snakes, with a large, globular sacculus. A phylogenetic analysis based on morphology recovers *Hypoptophis* as a sister taxon to *Aparallactus*. We also discuss the implications of our observations on the burrowing origin hypothesis of snakes.

KEYWORDS
Atractaspis, cranium, fang evolution, fossoriality, phylogeny, systematics

1 | INTRODUCTION

Snakes are the most successful clade of limbless squamates, with more than 3800 described extant species (Uetz et al., 2020). They have evolved fossoriality multiple times in different lineages throughout their evolutionary history (Greene, 1997). In fact, fossoriality has been discussed in relation to the origin of snakes themselves (e.g., Bellairs & Underwood, 1951; Da Silva et al., 2018; Walls, 1942; Yi & Norell, 2015), with early evolution in an aquatic environment being the other main opposing hypothesis in this "origin" debate (e.g., Caldwell & Lee, 1997). The preference for a largely secretive way

Sunandan Das and Jonathan Brecko have contributed equally and should be considered joint first authors.

of life in snakes has driven the appearance of an interesting array of adaptions in both their external and internal morphology (e.g., smaller eye and shorter tail, reduced dorsal scale rows, modified snout, trunk myoskeletal system, reinforced skull, etc. [Gans et al., 1978; Savitzky, 1983; Deufel, 2017; Olori & Bell, 2012; Lillywhite, 2014]). Skulls of fossorial animals often show striking incidences of heterochronic shifts (e.g., Kley, 2006; Strong et al. (2020)). Fossorial traits (or lack thereof) have been associated with significant differences in rates of speciation among snakes (Cyriac & Kodandaramaiah, 2018). While associating the snake "origin" to a specific mode of life, be it burrowing or marine, may be problematic (Caldwell, 2020), snakes nevertheless appear to have acquired fossorial adaptations quite early in their evolutionary history. Examples of such adaptations include the postulated fossorial/semifossorial-semiaquatic adaptation in the inner ear of Cretaceous *Dinilysia patagonica* (Palci et al., 2017; Yi & Norell, 2015), Cretaceous scolecophidian *Boipeba tayasuensis* (Fachini et al., 2020), and the presence of many extant fossorial snake clades or their common ancestors also in the Cretaceous, as revealed in time-calibrated phylogenies (e.g., Garberoglio et al., 2019; Zheng & Wiens, 2016). Therefore, we can expect to recover more Mesozoic and early Cenozoic snakes adapted to a semifossorial or fossorial way of life. Reliable inference on the paleoecology of such snakes calls for the need for extensive comparative data on the osteology of extant snakes, for which the actual ecology can be directly observed and confirmed. Including more observations from extant lineages often changes—or at least adds further insights into—the paleoecology of fossil taxa. The inner ear of *Dinilysia*, for instance, was regarded to be suggestive of a burrowing lifestyle by Yi and Norell (2015), but exploration of the inner ear of additional extant snakes by Palci et al. (2017) revealed the existence of a similar inner ear in a semiaquatic homalopsid snake living in mangrove burrows.

A strong predisposition for living and foraging in burrows, or even actively digging them (often with a modified snout), is seen not only in scolecophidians and multiple lineages of basal alethinophidians, but also in a number of colubroids. One such colubroid group is the family Atractaspididae, which consists of the subfamilies Aparallactinae and Atractaspidinae (Kelly et al., 2009; Zaher et al., 2019), or subfamilies Aparallactinae and Atractaspidinae within Lamprophiidae in other classification schemes, such as that of Pyron et al. (2013). Notably, these two subfamilies are always found to be the sister taxa to each other in all the aforementioned phylogenetic analyses. Atractaspidinae has two recognized genera, including the well-known, highly unusual venomous snakes of the genus *Atractaspis*, whereas eight genera are assigned to Aparallactinae (Portillo et al., 2018). These snakes are all fossorial, and their morphology, behavior, and predatory repertoire is suited for such an existence (Chippaux & Jackson, 2019; Marais, 2004; Spawls et al., 2018). Despite being more diverse in terms of both the number of taxa assigned and their morphology, aparallactines have not received as much attention from anatomists and functional morphologists as *Atractaspis* (e.g., Deufel & Cundall, 2003; Strong et al., 2020). Strong et al. (2020) described the cranial osteology thoroughly and discussed the evolution of burrowing adaptations in *Atractaspis irregularis*, but a similar detailed bone-by-bone description does not exist for any aparallactines. Bourgeois (1968) described the crania of some aparallactines and atractaspidines in her landmark contribution of African snake cranial osteology. The descriptive accounts and hand-drawn illustrations of Bourgeois (1968) focus mostly on cranial features that are visible externally, while some parts of the crania (especially, posterior braincase) are treated briefly. Hence, it is not always possible to extract all the anatomical information demanded by large phylogenetic matrices from that monograph. While Strong et al.'s (2020) contribution filled this gap largely for the atractaspidine *Atractaspis*, a serious knowledge gap continues to exist for aparallactines. In this context, we note that the knowledge of extinct caenophidians from sub-Saharan Africa is rather meager (Cadle, 1994; McCartney et al., 2014), but vertebral remains probably assignable to atractaspidids have been reported from the Pliocene Kanapoi formation (Head & Müller, 2020). Further paleoherpetological explorations are likely to reveal more atractaspidid, including aparallactine, material. Hence, material and osteological information from living species will be crucial for the identification of paleoherpetological material and inferences on paleoecology.

Here, we describe the cranial osteology of a central African aparallactine, *Hypoptophis wilsonii*, based on a female specimen collected in the Democratic Republic of Congo. This fossorial snake is distributed in the Democratic Republic of Congo and Zambia (Broadley & Cotterill, 2004). Rarely sighted in its natural habitat and even rarer in museum collections (Chippaux & Jackson, 2019), the biology of this species, including details of anatomy and natural history, remains unstudied. De Witte and Laurent (1947) were the first to recognize a close affinity of the monotypic *Hypoptophis* to genera currently assigned to Aparallactinae. Underwood and Kochva's (1993) cladistic analyses also recovered *Hypoptophis* to be close to genera allocated to Aparallactinae. To the best of our knowledge, no molecular phylogenetic studies have ever included *Hypoptophis*, perhaps due to the lack of availability of material. Therefore, while the allocation of *Hypoptophis* to Atractaspididae itself is generally accepted (e.g., Pyron et al., 2013), its specific phylogenetic affinity within the family is in need of a critical reappraisal.

As a step toward bridging the knowledge gap in aparallactine osteology, cranial elements of *Hypoptophis wilsonii* are described using micro-computed tomographic (μCT) scans of three specimens. The endocast of the inner ear was also prepared and described, as this region has proved to be of particular importance in drawing paleoecological inference (Palci et al., 2017; Palci et al., 2018; Yi & Norell, 2015). We discuss the fossorial adaptation in the cranium of *Hypoptophis* against the broader backdrop of fossorial traits in atractaspidids and Serpentes in general. Finally, we also infer the phylogenetic positioning of this taxon using cranial osteological data.

2 | MATERIAL AND METHODS

2.1 | Museum acronyms

AMNH—American Museum of Natural History (New York), CAS—California Academy of Science (San Francisco), FMNH—Field

Museum of Natural History (Chicago), FRIM—Forest Research Institute Malaysia (Kuala Lumpur, Malaysia), RBINS—Royal Belgian Institute of Natural Sciences (Brussels, Belgium), RMCA—Royal Museum of Central Africa (Tervuren, Belgium), TMM—Texas Memorial Museum (Austin), USNM—Smithsonian National Museum of Natural History (Washington), UMMZ—University of Michigan Museum of Zoology (Ann Arbor).

2.2 | Specimens

Three ethanol-preserved specimens of *Hypoptophis wilsonii* Boulenger, 1908, an adult female (RBINS-VER-REP 9712a), a juvenile female (RBINS-VER-REP 9712b), and an adult male (RBINS-VER-REP 9711), in the holding of the Royal Belgian Institute of Natural Sciences were CT-scanned for the present work. All specimens belong to the subspecies *Hypoptophis wilsonii katangae* (Müller, 1911). We have further scanned one specimen each from four additional aparallactines, namely *Aparallactus modestus*, *Chilorhinophis gerardi*, *Macrelaps microlepidotus*, and *Polemon christyi*, and one atractaspidine, *Atractaspis boulengeri*, from the collection of the Royal Museum of Central Africa and the Royal Belgian Institute of Natural Sciences. All scans performed for this study have been deposited in MorphoSource (https://www.morphosource.org/). Further comparative aparallactines and atractaspidid material (μCT scans) were obtained from MorphoSource (https://www.morphosource.org/) and Digimorph (http://digimorph.org/index.phtml) databases and from Strong et al. (2020) (an *Atractaspis irregularis*, the scan of which is also available on Digimorph). We also obtained scans of the skull of *Boaedon fuliginosus* as an outgroup for phylogenetic analyses, and some fossorial basal alethinophidians as comparative materials to study fossorial adaptations from MorphoSource and Digimorph, respectively. All used specimens are listed below (catalog numbers are in parentheses; M and D in superscript indicate MorphoSource and Digimorph, respectively; asterisk denotes the specimens scanned here for this work; MorphoSource ARK and DOI are given in Data S1):

Atractaspididae (Aparallactinae): *Amblyodipsas polylepis* (CAS:Herp:173555^{M}); *Aparallactus capensis* (CAS:H:11683^{M}); *Aparallactus modestus* (CAS:Herp:111865^{M}, RMCA-VER-R. 12^{*,M}); *Chilorhinophis gerardi* (CAS:H:159106^{M}, RMCA-VER-R. 1205^{*,M}); *Hypoptophis wilsonii* (RBINS-VER-REP 9711^{*,M}, 9712a^{*,M}, 9712b^{*,M}); *Macrelaps microlepidotus* (RMCA-VER-REP-81.06.R. 185^{*,M}); *Polemon christyi* (CAS:Herp:147905^{M}, RMCA-VER-R. 14373^{*,M}); *Xenocalamus bicolor* (CAS:Herp:248601^{M}).

Atractaspididae (Atractaspidinae): *Atractaspis aterrima* (AMNH:Herpetology:R-12352^{M}); *Atractaspis bibronii* (CAS:Herp:111668^{M}, UMMZ:Herps:209986^{M}); *Atractaspis boulengeri* (RBINS-VER-2045^{*,M}); *Atractaspis irregularis* (FMNH 62204^{D}); *Homoroselaps lacteus* (CAS:Herp:173258^{M}).

Lamprophiidae: *Boaedon fuliginosus* (CAS:Herp:85747^{M}).

Aniliidae: *Anilius scytale* (USNM 204078^{D}).

Anomochilidae: *Anomochilus leonardi* (FRIM 0026^{D}).

Cylindrophiidae: *Cylindrophis ruffus* (FMNH 60958^{D}).

Uropeltidae: *Rhinophis melanogaster* (FMNH 167048^{D}); *Uropeltis woodmasoni* (TMM M-10006^{D}).

Erycidae: *Eryx colubrinus* (FMNH 63117).

2.3 | CT-scanning

The specimens of the RBINS and RMCA collection used in this study were scanned at the μCT facility of the RBINS. All specimens, except one, were digitized using an EasyTom 150 (RX Solutions, Chavanod, France) with an aluminum filter at 10–30 W, 110 kV, 5.5–12.5 frames/s, 1440 projections per rotation and 11–19 μm isotropic voxelsize for head scans, and 32–45 μm isotropic voxelsize for full body scans. One specimen (*Chilorhinophis gerardi*) was scanned using an XRE UniTom (Tescan XRE, Ghent, Belgium) at 10–22 W, 75 kV, 150–400 ms frame rate, 1800 projections per rotation, and 9 and 22 μm isotropic voxelsize for head and full-body scan, respectively.

Segmentation of the scans was done using Dragonfly software, Version 4.1 for Windows (Object Research Systems (ORS) Inc, Montreal, Canada, 2020. Visualization of scans, including those obtained from databases, and preparation of figures were done with MeshLab (Cignoni et al., 2008).

2.4 | Terminology

The general terminology for the bones of the skull follows Cundall and Irish (2008), McDowell (2008), and Zaher and Scanferla (2012). We followed Evans (2016), Palci et al. (2017), and McDowell (2008) for the auditory system structures. When the identification of any bony structures in the present paper differs from the works cited above, appropriate references and reasons have been cited in the description of that particular structure. Identification of the sites of muscle origin and insertions on the cranial bones were done using the works by Pregill (1977), Cundall (1986), Tsuihiji (2007), Tsuihiji et al. (2012), and Das and Pramanick (2019).

2.5 | Phylogenetic analyses

For phylogenetic analyses, 61 cranial osteological characters were coded and scored for 14 Atractaspididae species and one species assigned to Lamprophiidae (see above). Criteria for inclusion and exclusion of characters are elaborated in Data S1 containing the character statements (sensu Sereno, 2007).

The deeper level of phylogeny and systematics of the superfamily Elapoidea remains unstable (e.g., Figueroa et al., 2016; Kelly et al., 2009; Pyron et al., 2013; Zaher et al., 2019). However, the monophyly of families Atractaspididae and Lamprophiidae are well corroborated. A lamprophiid—*Boaedon fuliginosus*—was used as an outgroup to root the tree.

Over the last few years, multiple simulation studies (O'Reilly et al., 2016; O'Reilly et al., 2018; Puttick, O'Reilly, Oakley, et al., 2017; Puttick, O'Reilly, Tanner, et al., 2017; Vernygora et al., 2020; Wright & Hillis, 2014) have consistently demonstrated the superiority of Bayesian Inference implementation of Markov k-states (Mk) models (Lewis, 2001) for discrete, anatomical data over Parsimony and Maximum Likelihood. Probabilistic methods allow for incorporation of

more information in the analyses, as even homoplasy and autapomorphy can contribute to better estimation of branch lengths and tree topology. Bayesian implementations have the added advantage of taking uncertainty into account by drawing from a large posterior distribution of trees instead of giving a point estimate. The data matrix was analyzed in MrBayes 3.2.6 (Ronquist et al., 2012) to infer a Bayesian Inference phylogeny. Some of the characters in the data matrix were ordered (see Data S1). To check for the effect of ordering on topology, we also ran an analysis with all characters unordered. The "coding" was set as "variable" and not "informative," as we have coded autapomorphies as well. The number of both chains and runs was set to four. The number of generations was initially set to 10,000,000, but we used the "stopval" and "stoprule" commands to stop the analyses once the average standard deviation of split frequencies fell below 0.01. Sampling was done every 500 generations. The first 25% of trees were cast off as burn-in. Chain convergence was also checked with Tracer 1.7 (Rambaut et al., 2018). Trees were visualized with FigTree 1.4.4 (https://github.com/rambaut/figtree/).

For the sake of comparison, we also inferred phylogenies using Maximum Parsimony from both the ordered and unordered data matrices with PAUP 4* Version 4.0a (GUI for Mac OSX; Swofford, 2003). The branch and bound algorithm were used to search for both the most parsimonious tree(s) and for bootstrap analyses. Multiple states of the same character for any taxa were treated as polymorphisms. Branch support was checked with 100 bootstrap replicates. Characters were given equal weights.

3 | RESULTS

3.1 | Cranial osteology

3.1.1 | Snout complex

This part consists of a single premaxilla and a pair of nasals, septomaxillae, and vomers (Figure 1).

Premaxilla

An A-shaped bone when seen from above and below (Figure 2a,b). The anterior end is projected forward, with a rounded outline, depressed dorsally (Figure 2d), and produced anteriorly and somewhat ventrally. The ascending process is triangular, with its anterior surface having a sigmoid curvature in the lateral view (Figure 2c,d). The posterior surface of the ascending process bears a transverse furrow, which divides the rear surface into an upper, caudally directed, tapering end and a lower, wide, nodular region. The posterior surface of the ascending process remains closely associated with the nasals. The transverse processes are large, almost straight along the outer edge and directed backward. However, on the inner edge of the transverse process, there is a slight, triangular, upturned projection that is concave below—this is most prominent in the adult male (RBINS-VER-REP 9711) specimen. The caudal end of the transverse process is proximate to the anterior end of the maxilla, and it seems likely that

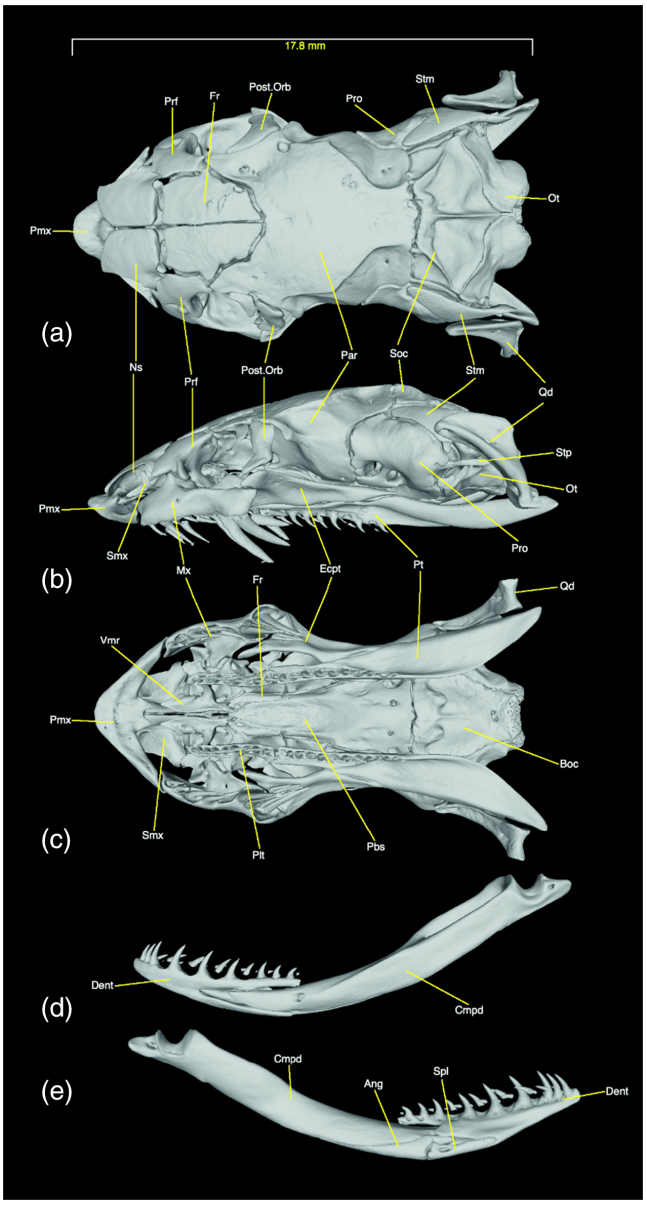

FIGURE 1 *Hypoptophis wilsonii* (RBINS-VER-REP 9712a), μCT-reconstruction of the cranium of an adult female. (a) Dorsal, (b) lateral (left side), (c) ventral views, (d) lateral view of the left mandible and (e) medial view of the left mandible. Length of the cranium was measured from the end of the atlantal flange to the premaxillary tip. Ang, angular; Boc, basioccipital; Cmpd, compound bone; Dent, dentary; Ecpt, ectopterygoid; Fr, frontal; Post.Orb, postorbital (fractured on the left side in this specimen); Mx, maxilla; Ns, nasal; Ot, otoccipital; Plt, palatine; Par, parietal; Pbs, parabasisphenoid; Pmx, premaxilla; Prf, prefrontal; Pro, prootic; Pt, pterygoid; Qd, quadrate; Soc, supraoccipital; Spl, splenial; Stm, supratemporal; Stp, stapes; Vmr, vomer

they form a loose saddle joint in life to reinforce the snout. The lateral corner of the caudal end of the transverse process is twisted upward (Figure 2d), which can fit into a shallow fossa on the anterolateral end of the maxilla. The maxillary rostral end, in turn, can be accommodated in a concavity just medial to the aforementioned, upwardly

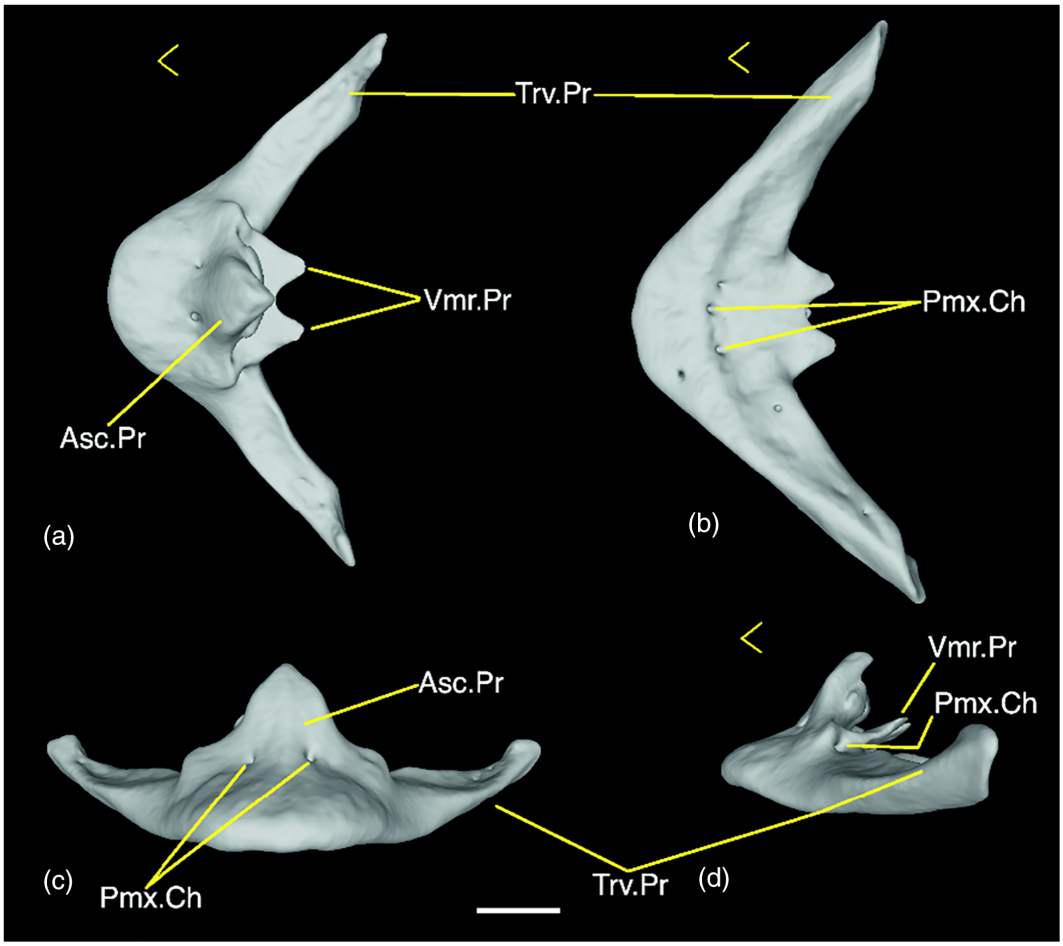

FIGURE 2 *Hypoptophis wilsonii* (RBINS-VER-REP 9712a), premaxilla. (a) Dorsal, (b) ventral, (c) anterior, and (d) lateral views. Asc.Pr, ascending process; Pmx.Ch, premaxillary channel; Trv.Pr, transverse process; Vmr.Pr, vomerine process. Scale bar, 1 mm. Arrowhead points to the rostral end of the cranium

twisted lateral corner of the caudal end of the transverse process. The two caudally directed vomerine processes are small, triangular and are separated by a shallow, triangular gap (Figure 2a,b,d). The vomerine processes are separated from the anterior processes of the vomer by a gap virtually as wide as the vomerine processes themselves. The position and number of the openings of the premaxillary channels on the frontal and ventral surfaces of the premaxilla are intraspecifically variable. However, two openings dorsad and rostrad to the junction between the vomerine and transverse processes consistently perforate the base of the ascending process posterolaterally (Figure 2d). There are two minute nodular projections immediately above and in front of these openings on each side.

Nasal

The dorsal horizontal laminae of the nasals are well developed (Figure 3a,b). Anteriorly, the dorsal horizontal laminae of the two nasals diverge from each other in a wide V-shape. The posterior part of the dorsal lamina widens laterally and gradually. The posterolateral corner of the dorsal lamina extends posteroventrally as a process medial to the lateral lamina of the prefrontal. There is a concavity on this posteroventral process from the nasal dorsal lamina, which allows it to slide in medial to the anteriorly pointed midpoint of the prefrontal lateral lamina. The caudal extremity of this process bears a notch, which fits in an anterior medial projection of the prefrontal (Figures 3b,c,e and 25). The straight transverse caudal edges of the dorsal laminae of the nasals are separated from the frontals by a narrow gap. The medial vertical laminae of the nasals are adpressed to each other. The anterior ends of the medial vertical laminae also diverge from each other and are modified into an articular surface. The articulatory surface consists of an anteriorly concave area and a convexity below that for receiving the tapering upper end and the nodule ventrad to that on the posterior surface of the premaxillary ascending process, respectively (Figure 3d). The distal end of the vertical lamina widens and articulates extensively with the medial frontal pillars, the contact spanning almost the entire height of the latter structure (Figure 3e,f). In this species, the prokinetic or the nasofrontal joint is almost completely mediated by the nasal, with the role of the septomaxilla being minimized to a rather meager contact with the frontal subolfactory process (Figure 3f).

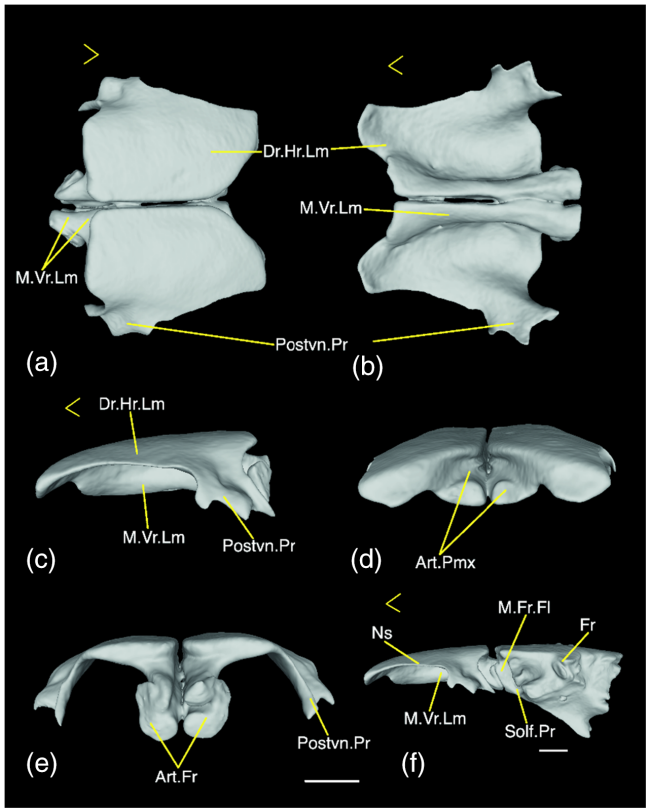

FIGURE 3 *Hypoptophis wilsonii* (RBINS-VER-REP 9712a), nasals. (a) Dorsal, (b) ventral, (c) lateral, (d) anterior, (e) posterior views, and (f) nasofrontal articulation. Art.Fr, articular surface for frontal; Art.Pmx, articular surface for premaxilla; Dr.Hr.Lm, dorsal horizontal lamina; Fr, frontal; M.Fr.Fl, medial frontal flange; M.Vr.Lm, medial vertical lamina; Ns, nasal; Postvn.Prposteroventral process; Solf.Pr, subolfactory process (of frontal). Scale bar = 1 mm. Arrowhead points to the rostral end of the cranium

Septomaxilla

This bone, together with the vomer, encloses the vomeronasal organ (Jacobson's organ). The anterior end of the septomaxilla, located dorsolateral and proximal to the premaxilla's vomerine processes, is pointed and anterolaterally emarginated (Figure 4a,b). Posterior to this, the septomaxilla markedly expands laterally and eventually curls up into a conchal process (Figure 4a,c). Caudal and medial to the conchal process, the septomaxilla forms the dorsal roofing and the anterior wall of the vomeronasal cupola (Figure 4b,c). Caudal to this part, the septomaxilla abruptly narrows to produce a slender, posteriorly, and somewhat ventrally directed medial process (Figure 4a,c). This posterior medial process contacts the nasal vertical lamina medially, and the frontal subolfactory process (lateral frontal flange) caudally. The anteromedial edge of the septomaxilla is rather upturned, while the posteromedial edge (the posterior medial process to be more specific) is rather ventrally twisted.

Vomer

Vomers articulate with the septomaxillae and complete the encasing of the vomeronasal organ. The ventral part of the vomer is boat-shaped, with the medial and lateral laminae meeting each other ventrally along a longitudinal keel (Figure 5a,d). The pointed anterior process of the vomer remains separated from the vomerine processes of the premaxilla by a gap. Dorsal to the boat-shaped ventral part, the vomer expands dorsally and laterally into an anteriorly and ventrally open dome, which, in conjunction with the septomaxilla, houses the vomeronasal organ (Figure 5a,c–f). The posterodorsal roof of this dome-shaped part is fenestrated by multiple foramina for the vomeronasal (CN I) nervelets (Figure 5c). The ventrally located vomeronasal fenestra is crescent-shaped. The posterior rim of the vomeronasal fenestra has a small posteroventrally directed projection. The interchoanal septum is deeply notched to produce a dorsal and ventral process (Figure 5a, b). The wide base of the ventral process, produced posteriorly as a small protuberance, is perforated by a large foramen (Figure 5a,b,f). As is the usual state in the Colubroidea (Cundall & Irish, 2008), the medial suture between the septomaxilla and the vomer leaves no gap, as is typical for basal alethinophidians.

3.1.2 | Braincase and circumorbital bones

Frontal, prefrontal, postorbital, parietal, prootic, otoccipital, supraoccipital, parabasisphenoid, and basioccipital compose the braincase and circumorbital elements (Figure 1). Of these, the frontal, prefrontal, postorbital, prootic, and otoccipital are paired elements.

Prefrontal

The prefrontal articulates dorsomedially with the frontal, anteromedially with the nasal, and ventrally with the maxilla. The posterodorsal corner of the prefrontal projects out into a small supraorbital process which is proximal to the supraorbital process of the parietal, and might be in a loose contact in life. The midpoint of the anterior margin of the prefrontal lateral lamina projects rostrally like the apex of a triangle (Figure 6a). The orbital lamina is distinctly concave, and there is a horn-shaped mediodorsally curved projection jutting out from its ventromedial edge (Figure 6b–d), akin to a projection at the same site in pythons labeled as medial extension by Frazzetta (1966). A lacrimal foramen perforates the orbital lamina that finally opens anteriorly with a ventromedially widened foramen (Figure 6c,d). The part of the prefrontal ventral lamina constituting the floor of the lacrimal foramen is little convex ventrally, but the lateral part articulating with the ascending process of the maxilla is concave to receive the process from the maxilla. Caudal to this concavity, the posterolateral corner, where the orbital, lateral and ventral laminae meet each other, gives rise to a small, posteroventrally directed, linguiform lateral foot process (Figure 6a,d). Rostrad to the maxillary ascending process, the anteroventral corner of the lateral lamina also projects ventrally. Enclosed between the lateral and orbital laminae, there is an articular surface clasping the prefrontal process from the frontal (Figure 6b,c). Along the dorsomedial edge of the orbital lamina, there are two articulatory facets (Figure 6b), which abut their counterparts on the frontal below and

behind the prefrontal process. Above the anterior lacrimal foramen is an anterior medial projection, which fits in a notch at the posterolateral corner of the nasal horizontal lamina (Figure 6b,c). The prefrontal in *Hypoptophis* does not have any dorsal lappet, and lacks a distinct conchal process.

Frontal

The paired frontals meet along the dorsal midline in a straight suture (Figure 7a). The dorsal horizontal lamina of the frontals narrows posteriorly. Posteriorly, the dorsal horizontal laminae of the frontals meet the parietal in a posteriorly concave (in dorsal view) suture (Figure 1a). The dorsolateral surface of the caudal half of the frontal is an articular surface for the supraorbital process of the parietal (Figure 7e,f). At the lateral midpoint of the frontal's dorsal horizontal lamina, where the prefrontal and supraorbital process of the parietal almost come into contact (possibly meet in life), there is a small triangular projection (Figure 7a). A stout lateral projection from the anterolateral surface of the frontal, called the prefrontal process, is lodged between the lateral and orbital laminae of the prefrontal (Figure 7b–d). There are two additional smaller articulatory facets for the prefrontal, one behind and the other below the prefrontal process (Figure 7e). From the anterior medial surface of each frontal, a medial frontal flange or pillar originates, which fuses with the frontal subolfactory process (Rieppel, 2007) without leaving any trace of a suture (Figure 7c,d). The orbital laminae of the frontals, which form the medial wall of the eye, are ventromedially oriented. The medial frontal flanges from the two frontals meet each other along their medial surface. The anterior surfaces of the medial frontal flanges expand dorsolaterally and together form an extensive articular surface (Figure 7c), concave and somewhat back-slanted, for the nasal. There is no septomaxillary process projecting out of the frontal subolfactory process. Instead, the septomaxilla's posterior medial extension contacts the frontal subolfactory process (however, the septomaxilla plays only a minor role in the nasofrontal joint in this species). In *Hypoptophis*, the frontal subolfactory processes form well-developed ventral laminae which meet each other in a straight suture (Figure 7b). This ventral surface sits almost flat on the dorsal surface of the parasphenoid rostrum, which is possible because the intertrabecular crest on the latter is a wide, flat surface. A sharp ridge delineates the edge where the ventral or subolfactory lamina meets the ventromedially descending orbital lamina (Figure 7b). Between this ridge and the lateral margin of the parasphenoid rostrum runs the trabecula cranii groove. Caudally, this ridge gives rise to what Strong et al. (2020) call a posteroventral process (Figure 7b,e,f), which closely approaches—albeit may not always touch—another process coming from the parietal below the optic foramen. Dorsad to the posteroventral process, the orbital lamina of the frontal is a little concave for the optic foramen.

Parietal

The parietal is a large, conspicuous dorsal and lateral element encasing the brain. The dorsal horizontal lamina of the parietal meets the frontal in a posteriorly emarginated suture anteriorly (Figure 1a). The anterolateral ends of the parietal send stout, anteriorly tapering supraorbital processes embracing the frontal from both sides, constituting the dorsal bony roofing for the orbit and acting as the site of articulation for the postorbital (Figure 8a–c). The rostral ends of the supraorbital processes almost touch the prefrontal (and likely remain in a loose contact indeed, though probably not in all the specimens). A pronounced postorbital ridge continues posteroventrally for some length from that supraorbital process (Figure 8a, c). The conspicuous adductor ridges (possibly for fibers of the heads of M. levator anguli oris and/or M. adductor mandibulae externus medialis-profundus [Das & Pramanick, 2019]) first extend straight caudad along the dorsolateral surface of the parietal, the ridge from one side being parallel to that on the contralateral side. Then they continue posteromedially, thus bridging the gap between them to a large extent, before running

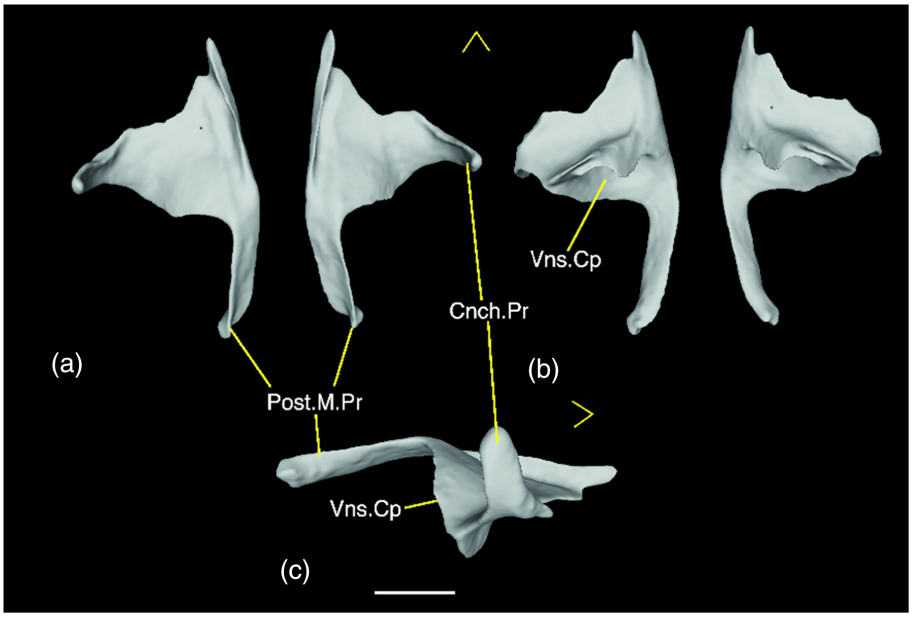

FIGURE 4 *Hypoptophis wilsonii* (RBINS-VER-REP 9712a), septomaxillae. (a) Dorsal, (b) ventral and (c) lateral view (right septomaxilla). Cnch.Pr, conchal process; Post.M.Pr, posterior medial process; Vns.Cp, housing of vomeronasal cupola. Scale bar = 1 mm. Arrowhead points to the rostral end of the cranium

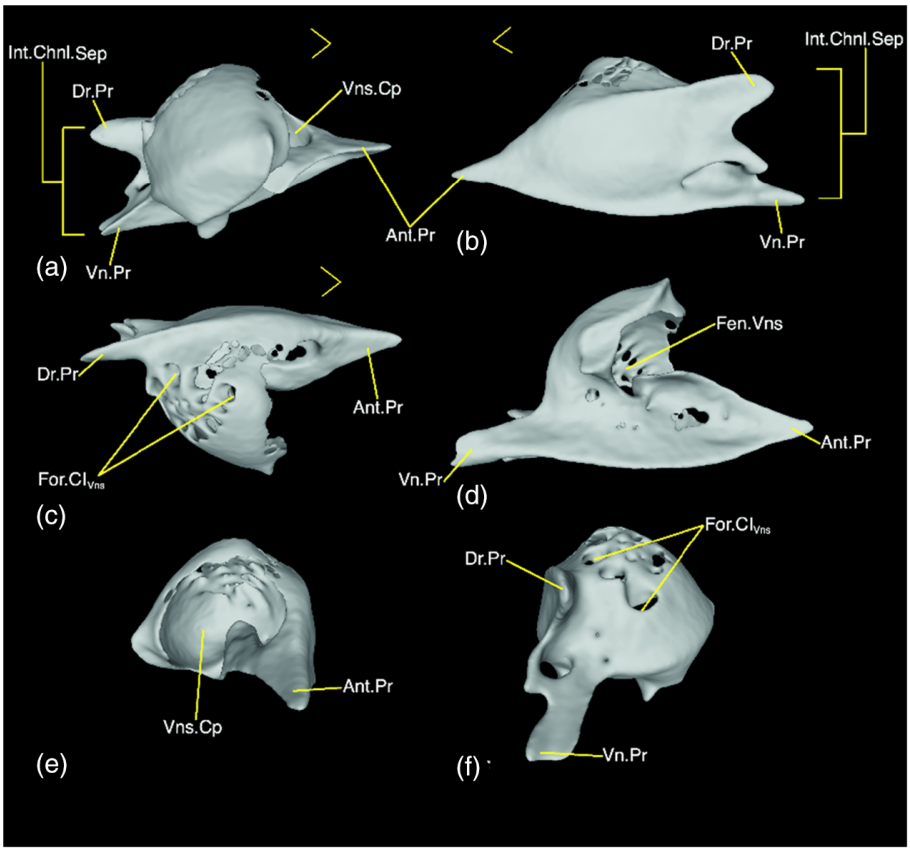

FIGURE 5 *Hypoptophis wilsonii* (RBINS-VER-REP 9712a), vomer. (a) Lateral, (b) medial, (c) dorsal, (d) ventral, (e) anterior, and (f) posterior views. Ant. Pr, anterior process; Dr.Pr, dorsal process (of the interchoanal septum); Fen.Vns, vomeronasal fenestra; For.Cl$_{Vns}$, foramina for vomeronasal nervelets; Int.Chnl.Sep, interchoanal septum; Vn.Pr, ventral process (of the interchoanal septum); Vns. Cp, housing of the vomeronasal cupola. Scale bar, 1 mm. Arrowhead points to the rostral end of the cranium

straight caudad again in parallel, this time with a much narrower gap separating them (Figure 8a). This ridge is somewhat less conspicuous in the juvenile specimen. Ventrolateral to the adductor ridge, lateral lamina of the parietal descends down to meet the parabasisphenoid. This laterally descending lamina turns a little medial anteriorly and forms the orbital lamina, the posteromedial bony wall for the orbit. There is a strong embayment at the lower aspect of the orbital lamina for the optic foramen (Figure 8c). Ventral to this recess is a slender anteriorly directed process which either contacts (RBINS-VER-REP 9711) or remains just separated from the posteroventral process from the frontal, thus either completely or almost excluding the parabasisphenoid from the ventral border of the optic foramen. Posterior to the orbital lamina, the laterally descending lamina bulges laterally. In keeping with this lateral bulging, a large depression can be observed on the inner surface, which is possibly caused by the cerebral hemispheres (Allemand et al., 2017; Figure 8b). There is a ridge demarcating the depressions of the left and right sides (corresponding to the two cerebral hemispheres), running along the ventral midline of the dorsal-horizontal lamina of the parietal. Two small but deep depressions, located abreast, are on the ventral surface of the dorsal horizontal lamina where the latter meets the supraoccipital (Figure 8b). Posteromedially, the parietal has a posteriorly convex medial parietal pillar (Zaher & Scanferla, 2012) which articulates with the prootic behind (Figure 8d). The ventral aspect of this medial parietal pillar has a small foramen in RBINS-VER-REP 9712a for the entry of the cid-nerve (CN V_4) that innervates the constrictor internus dorsalis group of muscles. In RBINS-VER-REP 9711 and 9712b, however, cid-nerve initially run rostrad, after leaving the prootic, within the parietal-parabasisphenoid suture before coming onto the parietal entirely via a slight notch in the ventral margin of the latter. In this species, the cid-nerve runs along a gutter located along the ventromedial edge of the parietal for some length (Figure 8d) before finally leaving the braincase through a small foramen in the parietal, caudad to the secondary anterior opening of the vidian canal. The secondary anterior opening of the vidian canal is either completely in the parietal (viz. in RBINS-VER-REP 9712a, left side of head in RBINS-VER-REP 9711; Figure 8c) or at the parietal-parabasisphenoid suture (in RBINS-VER-REP 9712b and on the right side of the head of RBINS-VER-REP 9711), through a deep recess in the parietal ventral margin. When that opening is entirely within the parietal, the anterior end of the intracranial vidian canal also comes up on the ventromedial edge of the parietal.

Postorbital

This bone forms the dorsolateral rim of the orbit caudally (Figure 1a, b). It was homologized to the jugal of the lizards by Palci and Caldwell (2013), but this issue still remains contentious (Cundall, 2020). Therefore, we use the traditional identification for this element (e.g., Cundall & Irish, 2008). The anterior margin of the postorbital is recessed in a semilunar shape. The posterior edge, however, is more irregular. The postorbital articulates with the supraorbital process and the postorbital ridge of the parietal. The left postorbital is broken in RBINS-VER-REP 9712a.

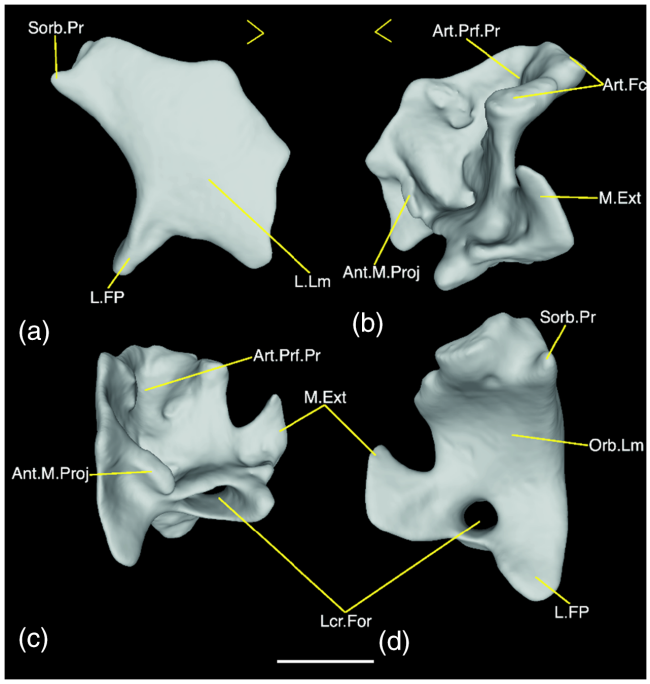

FIGURE 6 *Hypoptophis wilsonii* (RBINS-VER-REP 9712a), right prefrontal. (a) Lateral, (b) medial, (c) anterior, and (d) posterior views. Ant.M.Proj, Anterior medial projection; art.Fc, articular facet; art.Prf.Pr, articular surface for the prefrontal process (from frontal); L.FP, lateral foot process; (l) Lm, lateral lamina; Lcr.For, lacrimal foramen; (m) Ext, medial extension; Orb.Lm, orbital lamina; Sorb.Pr, supraorbital process. Scale bar = 1 mm. Arrowhead points to the rostral end of the cranium

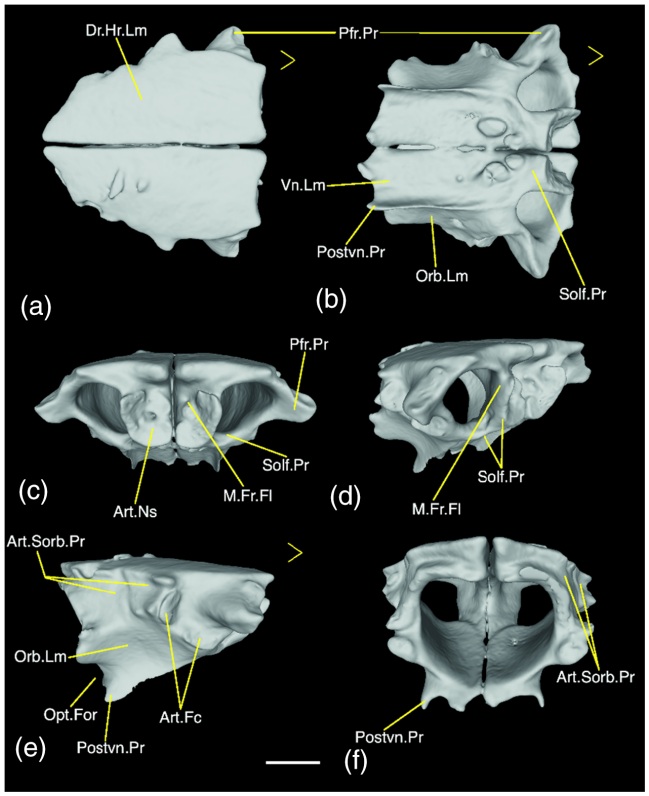

FIGURE 7 *Hypoptophis wilsonii* (RBINS-VER-REP 9712a), frontals. (a) Dorsal, (b) ventral, (c) anterior, (d) anterolateral, (e) lateral, and (f) posterior views. Art.Fc, articular facet; Art.Ns, articular surface for nasal; Art.Sorb.Pr, articular surface for the supraorbital process of the parietal; Dr.Hr.Lm, dorsal horizontal lamina; M.Fr.Fl, medial frontal flange; Opt.For, optic foramen; Orb.Lm, orbital lamina; Pfr.Pr, prefrontal process; Postvn.Pr, posteroventral process; Solf.Pr, subolfactory process; Vn.Lm, ventral (subolfactory) lamina. Scale bar—1 mm. Arrowhead points to the rostral end of the cranium

Parabasisphenoid

The dermal parasphenoid and the chondrocranial basisphenoid fuse in snakes to form the parabasisphenoid. The wider posterior part of the basisphenoid is ventrally convex, with a concave dorsal surface. There is a shallow sella turcica and a well-developed dorsum sellae that partially roofs the sella turcica (Figure 9a). On the ventral surface, the posterior opening of the vidian canal perforates the basisphenoid, close to the suture with the prootic (Figure 9b). There is a striking asymmetry between the posterior opening of the vidian canal on the left and right side of the head. The opening on the left side of the head is much larger (to the extent of producing an emargination on the left lateral edge of the basisphenoid) than the one on the right (Figure 9b). This kind of asymmetry is also observed in Pythonidae and Boidae (Underwood, 1967). Most aparallactines examined by us show a similar asymmetry in left versus right posterior vidian canal opening diameter. The canal that commences at this opening bifurcates inside the basisphenoid. The bifurcation results in a lateral, longer, and narrower vidian canal proper and a median, short and larger (especially the left side, in keeping with the larger foramen on the ventral surface of that side) opening, just lateral to the sella turcica. After a short distance, the vidian canal opens inside the braincase through the primary anterior opening of the vidian canal (Rieppel, 1979; Figure 1a), proximal to the anterior end of the base of the short, triangular clinoid process (Figure 1c). Along the anterior slope of the clinoid process lies a gutter along which the cid-nerve runs for a short distance, roofed by the parietal (except in RBINS-VER-REP 9712a, where the cid-nerve directly enters the parietal via a foramen), before extending rostrad along another gutter on the ventromedial surface of the parietal. The palatine branch of the facial (CN VII) nerve runs through the vidian canals, emerges intracranially through the primary anterior opening of the vidian canal, then runs forward along a gutter formed first by the basisphenoid to finally continue on the parietal. The palatine branch of the VII nerve eventually leaves the braincase via a secondary anterior opening of the vidian canal perforating the ventral border of the parietal. A small anterior abducens (CN VI) nerve foramen is located lateral to the dorsum sellae, at the base of the clinoid process (Figure 9a). The posterior abducens foramen, small like the anterior one, is located slightly caudad to the anterior foramen (Figure 9a). The cultriform process or parasphenoid rostrum of *Hypoptophis* gradually tapers anteriorly and is rather concave on the ventral surface. The intertrabecular crest is a wide flat surface, rather than a "crest," as the cultriform process is relatively wide in this species (Figure 9a).

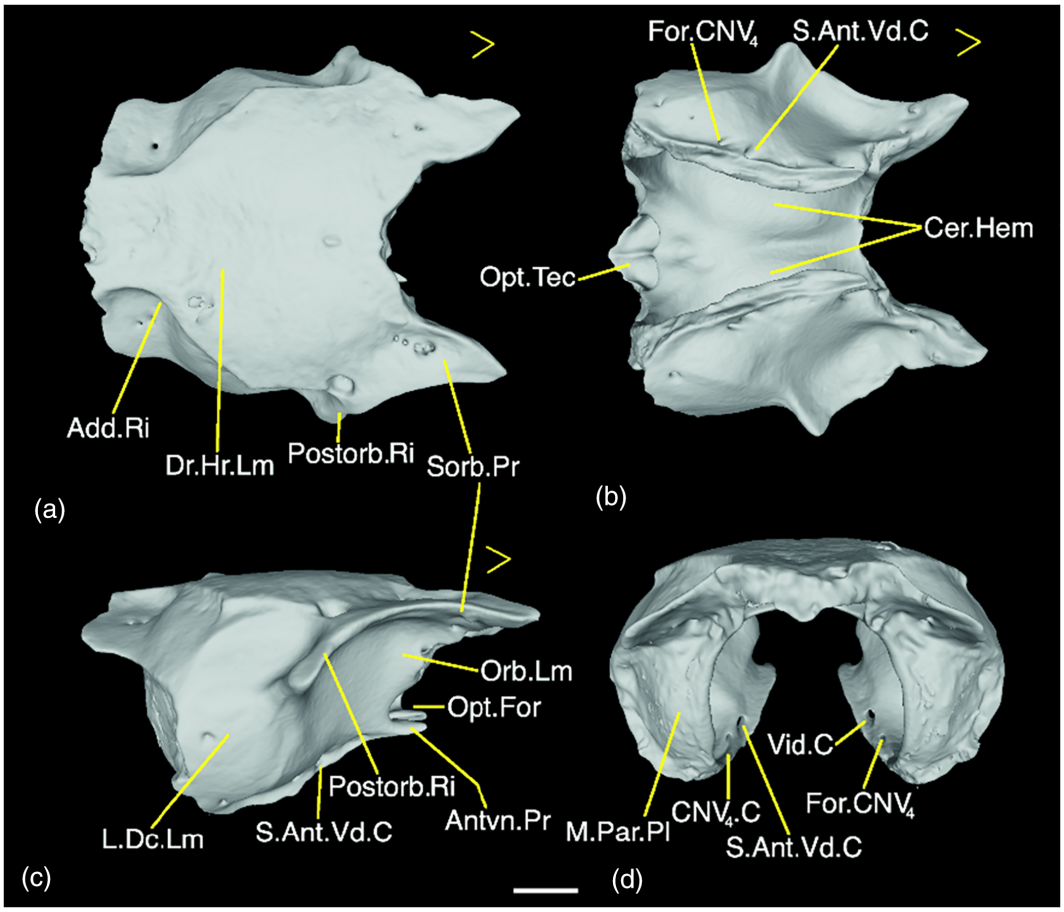

FIGURE 8 *Hypoptophis wilsonii* (RBINS-VER-REP 9712a), parietal. (a) Dorsal, (b) ventral, (c) lateral, and (d) posterior views. Add. Ri, adductor ridge; antvn.Pr, anteroventral process; Cer.Hem, depression indicating the location of the cerebral hemispheres; CNV_4.C, cid-nerve canal; Dr.Hr. Lm, dorsal horizontal lamina; For.CNV_4foramen of the cid-nerve; L.Dc.Lm, lateral descending lamina; M.Par.Pl, medial parietal pillar; Opt.For, optic foramen; Opt.Tec, depression indicating the location of the optic tectum; Orb.Lm, orbital lamina; Postorb.Ri, postorbital ridge; S.Ant.Vd.C, secondary anterior opening of the vidial canal; Sorb.Pr, supraorbital process; Vid.C, vidian canal (only the anterior end). Scale bar = 1 mm. Arrowhead points to the rostral end of the cranium

Prootic

The prootic is a complex bone of the lateral braincase. It is the anterolateral component of the otic capsule, and is hollowed out for housing parts of the inner ear, namely anterior and lateral ampulla, lagena and parts of the sacculus, anterior and lateral semicircular canals and utriculus (Figures 10c,d and 23d,e, inset). The anterior wall, not visible in the external view, articulates with the medial parietal pillar. The wall continues further medially and ventrally, dorsal to the trigemino-facialis chamber (in the usage of Rieppel, 1979), to form part of the housing of the inner ear. There is a deep U-shaped embayment on the medial wall's margin, which, together with a similar recess on the otoccipital, forms the foramen for the posterior ramus of the vestibulo-acoustic (CN VIII) nerve (Figure 10c,d). A small foramen for the anterior ramus of the VIII nerve is located rostrad to the aforementioned foramen (Figure 10c). The trigemino-facialis chamber is situated beneath the housing of the inner ear (Figure 10c). Laterally, a bony strut, usually labeled as the laterosphenoid (e.g., Cundall & Irish, 2008; Kamal & Hammouda, 1965) although called the alethinophidian bridge following McDowell (1987, 2008) here, divides the trigeminal foramen into an anterior trigeminal foramen for the passage of the maxillary ramus (CN V_2) of the trigeminal (CN V) nerve and a posterior trigeminal foramen through which the mandibular ramus (CN V_3) of the V nerve emerges (Figure 10a). The term "laterosphenoid" is in usage for a nonhomologous (with respect to that of snakes) structure in front of the trigeminal foramen in the fossil and extant archosaurs (Brusatte, 2012; Clark et al., 1993; McDowell, 2008; Rieppel, 1976). Hence, Clark et al. (1993) called for a novel term to be applied for the structure in snakes, which McDowell's (2008) "alethinophidian bridge" serves. Notably, Gauthier et al. (2012) termed the same structure as "ophidiosphenoid," but McDowell's term appears to be more appropriate, as this trait mainly characterizes alethinophidians. A foramen for the conveyance of the cid-nerve (CN V_4) pierces the anteroventral border of the anterior trigeminal foramen and eventually opens toward the bottom of the prootic anterior wall; the cid-nerve leaves the prootic here and enters into the parietal. A small foramen for the palatine branch of the facial (CN VII) nerve is located on the floor of the posterior trigeminal foramen. The palatine branch of the VII nerve exits the prootic via another

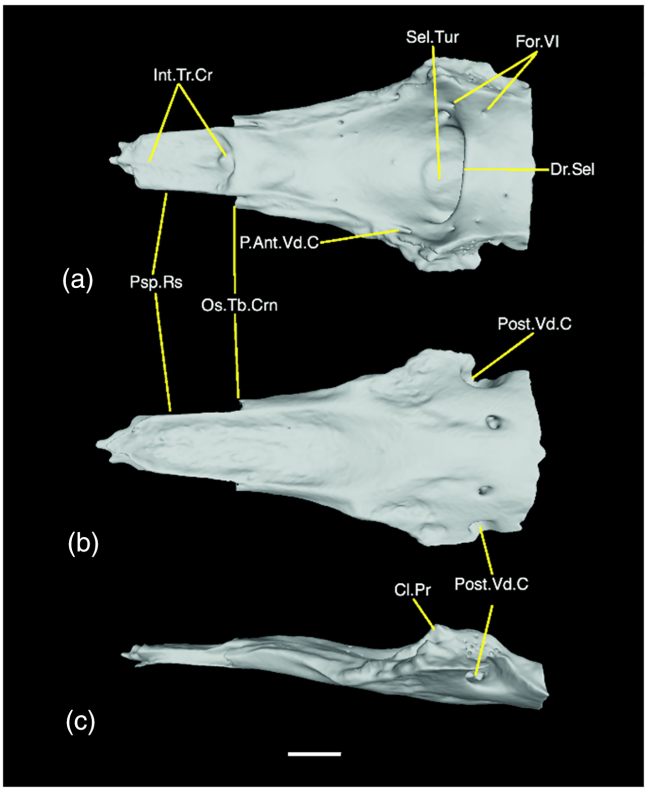

FIGURE 9 *Hypoptophis wilsonii* (RBINS-VER-REP 9712a), parabasisphenoid. (a) Dorsal, (b) ventral and (c) lateral views. Cl.Pr., clinoid process; Dr.Sel, dorsum sellae; For.VI, abducens nerve foramen; Int.Tr.Cr., intertrabecular crest; Os.Tb.Crn, ossified end of the trabeculae cranii; P.Ant.Vd.C, primary anterior opening of the vidian canal; Post.Vd.C, posterior foramen of the vidian canal; Psp.Rs, parasphenoid rostrum; Sel.Tur, sella turcica. Scale bar—1 mm. Arrowhead points to the rostral end of the cranium

small foramen beneath the posterior trigeminal foramen and then runs along an anteroventrally directed gutter to the posterior opening of the vidian canal (Figure 10a). The foramen for the hyomandibular branch of the VII nerve opens on the roof of the posterior trigeminal foramen (Figure 10a; in the male, the foramen opens outside of the posterior trigeminal foramen, posterior to the latter, on the right prootic). The prootic bulges lateral to the juxtastapedial recess. The crista prootica forms a distinct crista circumfenestralis dorsalis. The supratemporal attaches on the dorsolateral surface of the prootic (Figure 10b). Lateroventral to this attachment, there is an indistinct, longitudinal ridge formed of some feeble bumps on the prootic.

Supraoccipital

The supraoccipital is an irregular pentagon-shaped bone when viewed from above, with the concave anterior margin contacting the parietal, and the posterior apex being wedged between the otoccipitals. There are three crests on the dorsal surface of the bone, namely a sagittal crest and two anteromedially directed adductor crests, running from the posterolateral corner of the supraoccipital to the adductor crest on the parietal (Figure 11a). The lateral edges of the adductor crests serve as the origin for the head of the M. adductor mandibulae externus medialis-profundus (this muscle originates from dorsal to supratemporal, often supraoccipital, in caenophidians [Das & Pramanick, 2019]), and the posterior edges of the crest receive the slip of the M. spinalis capitis. On the ventral surface of the supraoccipital, there are two triangular median flanges with their apex pointing ventrally (Figure 11b,c,e). These median flanges articulate with the medial walls of the prootic and the exoccipital, thus completing the encapsulation of the inner ear dorsomedially. Each median flange is perforated by an upward directed endolymphatic foramen (Figure 11c).

Otoccipital

The otoccipital forms the dorsal roofing of the foramen magnum. Anteriorly, the otoccipitals participate in forming the juxtastapedial recess and the fenestra vestibuli. On the dorsolateral surface of the bone, there is a posteroventrally directed crest which continues to the paroccipital process, a protuberance posterodorsal to the juxtastapedial recess (Figure 12a,b). The posterior surface of the crest and the paroccipital process likely serve as the insertion site for parts of the M. longissimus capitis (Pregill, 1977; Tsuihiji, 2007). A ventrally directed digitiform process from the otoccipital complements the crista circumfenestralis dorsalis formed by crista prootica. The crista tuberalis, which forms the crista circumfenestralis ventralis, is well-developed and obstructs the visibility of the crista interfenestralis in the lateral view, and therefore we regard *Hypoptophis* to have a Type 4 (i.e., the most developed) crista circumfenestralis according to the scales of development of this structure as defined by Palci and Caldwell (2014). The crista interfenestralis is an anteroventrally slanted bony lamina, with its flat rostral surface facing somewhat medially, which forms the posteroventral boundary of the fenestra ovalis. The Wever's facet, a narrow contact surface for the flat posterior edge of the stapedial footplate, is located immediately dorsal to the crista interfenestralis (Figure 12b). The periotic or perilymphatic sac is located medial to the crista interfenestralis (Figure 12d). The periotic sac opens laterally via a periotic foramen dorsal to the roof of the recessus scalae tympani (Figure 12b), behind the crista interfenestralis. The apertura lateralis recessus scalae tympani is situated ventral to the periotic foramen. The recessus scalae tympani opens inside the braincase through the apertura medialis recessus scalae tympani, located close to the suture of the otoccipital and basioccipital (Figure 12b). The floor of the recessus scalae tympani is formed completely by the otoccipital, with no contribution from the basioccipital. Between its lateral and medial laminae, the otoccipital houses parts of the sacculus, the lateral and posterior semicircular canals, and the periotic sac and thus completes the otic capsule together with the prootic and supraoccipital (Figures 12c,d and 23d,e, inset). A jugular foramen pierces the otoccipital behind the crista tuberalis through which the glossopharyngeal (CN IX) and the vagus (CN X) nerves pass (Figure 12a,c; occasionally one CN IX ramus seems to exit through the crista tuberalis, as in the adult and juvenile females). A pair of openings, likely for the hypoglossal (CN XII), are located just behind the jugular foramen, separated from the latter by a thin, bony lamina (Figure 12a,c). Three smaller foramina, through

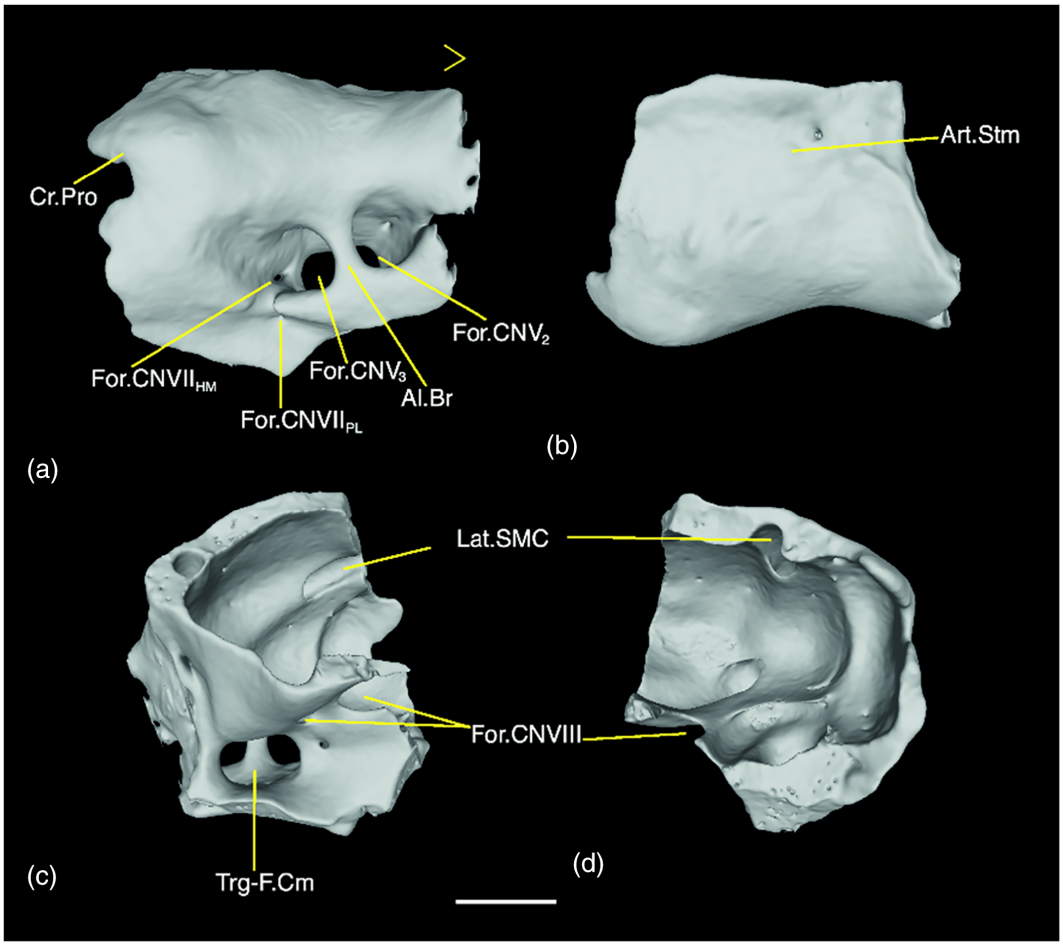

FIGURE 10 *Hypoptophis wilsonii* (RBINS-VER-REP 9712a), right prootic. (a) Lateral, (b) dorsal, (c) medial, and (d) posterior views. Al.Br., alethinophidian bridge; Art.Stm, articular surface for the supratemporal; Cr.Pro, Crista prootica (forming crista circumfenestralis dorsalis); For.CNV$_2$, foramen for the maxillary branch of the trigeminal nerve; For.CNV$_3$, foramen for the mandibular branch of the trigeminal nerve; For.CNVII$_{HM}$, hyomandibular branch of the facial nerve; For.CNVII$_{PL}$, palatine branch of the facial nerve; For.CNVIII, foramen for the posterior branch of the vestibulo-acoustic nerve; Lat.SMC, lateral semicircular canal; Trg-F.Cm, trigemino-facialis chamber. Scale bar—1 mm. Arrowhead points to the rostral end of the cranium

which the posterior rami of CN XII might pass, are located near the base of the occipital condyle. There is a slight laterally projecting ridge below the jugular foramen which is continuous anteriorly with the ventral foot process of the crista interfenestralis (Zaher & Scanferla, 2012; McDowell, 2008 called it "tuberosity of processus interfenestralis"). The latter is a transversely oriented rectangular growth on the ventrolateral surface of the ectopterygoid, below the fenestra ovalis (Figure 12a,b); both this ridge and the ventral foot process of the crista interfenestralis are weakly developed in the juvenile. The otoccipital contributes to forming the lateral parts of the occipital condyle, with the basioccipital contribution in between, and this part consists of cancellous bone. There is a weak and short posteroventrally directed ridge on the lateral surface of the occipital condyle, which may be a homolog of the prominent tubercular structure seen at the same site in pythonids (McDowell, 1975). The atlantal flanges of the otoccipitals are well developed (Figure 12a) and slightly overlap the neural arch of the atlas vertebra.

Basioccipital

The basioccipital is an irregular hexagonal shield-shaped bone sutured to the parabasisphenoid's posterior edge, with the prootics along the anterolateral edges and the otoccipitals along the posterolateral margins. The wider anterior two-thirds of this posterior-most bone of the ventral braincase are ventrally convex, with a corresponding concavity on the dorsal surface (Figure 13a,b). There is a slight notch at the median point of the anterior border of the basioccipital, which receives a weakly developed triangular process from the parabasisphenoid posterior edge. Along the anterolateral border, there is a ridge which attains its maximal prominence at the angle where the anterolateral and posterolateral edges meet (Figure 13a,b). This is the basioccipital element of the spheno-occipital tubercle, below the ventral foot process of the crista circumfenestralis. The ridge and the tubercle are not clearly developed in the juvenile. The ridge continues along the anterior edge to merge in the median basioccipital process (Pregill, 1977 called it so in the colubrid *Coluber constrictor*). The two median basioccipital processes (Figure 13b), serving as the insertion

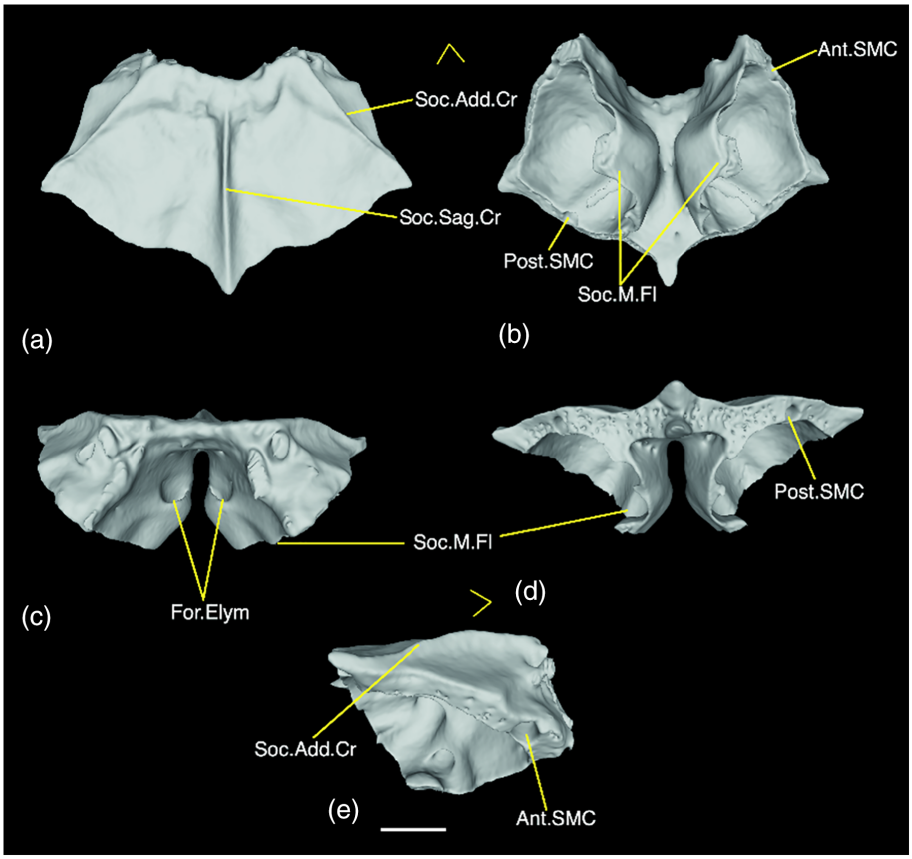

FIGURE 11 *Hypoptophis wilsonii* (RBINS-VER-REP 9712a), supraoccipital. (a) Dorsal, (b) ventral, (c) anterior, (d) posterior, and (e) medial views. Ant.SMC, anterior semicircular canal; For.Elym, endolymphatic foramen; Post.SMC, posterior semicircular canal; Soc.Add.Cr, supraoccipital adductor crest; Soc.M.Fl, supraoccipital medial flange; Soc.Sag.Cr, supraoccipital sagittal crest. Scale bar—1 mm. Arrowhead points to the rostral end of the cranium

site for the tendon of the M. rectus capitis anterior, pars ventralis (Pregill, 1977), are prominent and stub-like in adults, but not well-developed in juveniles, in which they exist merely as two convexities. A feeble longitudinal ridge originates between the median basioccipital processes, which subsides completely into the surface after running some distance caudad. This ridge is not developed in juveniles. The narrow caudal end of the basioccipital forms the median component of the occipital condyle. This part of the basioccipital is mostly cancellous, being more so in the adult and juvenile female specimens (RBINS-VER-REP 9712a and b). In the male specimen (RBINS-VER-REP 9711), the basioccipital is almost completely fused to the parabasisphenoid, leaving only a few traces of the suture that would persist in a normal condition.

3.1.3 | Palatomaxillary arch

The palatomaxillary arch is composed of paired maxilla, palatine, pterygoid, and ectopterygoid (Figures 1 and S9).

Maxilla

The rather short maxilla is a dentigerous bone. The anterolateral end is concave for receiving the end of the premaxillary transverse process (Figure 14a). On the dorsal surface, there is a triangular ascending process (Figure 14a–c), with its apex pointing dorsally and fitting into a concavity on the ventral surface of the prefrontal (Figure 1b). Medial to the apex of the maxillary ascending process, a triangular palatine process projects out in a ventromedial direction (Figures 14b–d and S9). The palatine process is just rostrad to the maxillary process of the palatine, and there might be only a loose contact between these elements. Together with the palatine process, the ascending process forms an articulatory surface for the prefrontal. The ectopterygoid process is almost confluent with the palatine process, with a slight ridge along the posterior border of the latter being the only demarcation between the two (Figure 14c, d). The medial edge of the ectopterygoid process is turned ventrally (Figure 14b). The maxilla bears four ungrooved recurved teeth, of which the anteriormost is the smallest, followed by a small one tooth-wide diastema and then a grooved, enlarged rear fang at the caudal end. The fang is about two times longer than the largest of the ungrooved teeth and, apart from the groove running down along its anterolateral surface, bears a feeble cutting edge along the distal half of its posterior surface. There are two alveoli for the fangs, and any one alveolus bears a functional fang at a time, with the fang that will replace the current one being positioned in close proximity to the unoccupied alveolus. These two alveoli are not fully abreast; the medial one is a little ahead of the lateral one, and thus, the location of the fang slightly differs depending on which of the alveoli is occupied by the currently functional fang. Besides the functional fang, there are three to four (more commonly four) replacement fangs in development.

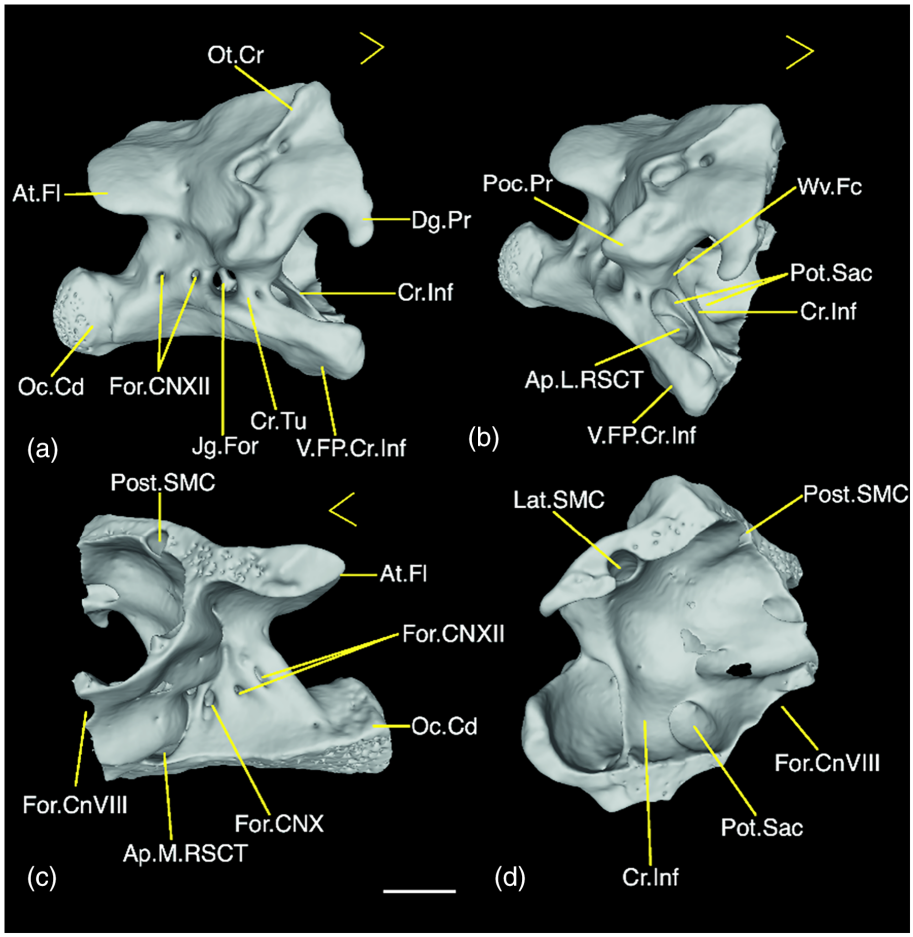

FIGURE 12 *Hypoptophis wilsonii* (RBINS-VER-REP 9712a), otoccipital. (a) Lateral, (b) anterolateral, (c) medial, and (d) anterior views. Ap.L.RSCT, apertura lateralis recessus scalae tympani; Ap.M.RSCT, apertura medialis recessus scalae tympani; At.Fl, atlantal flange; Cr.Inf, crista interfenestralis; Cr.Tu, crista tuberalis; Dg.Pr, digitiform process (completing the crista circumfenestralis dorsalis formed primarily of the crista prootica of the prootic); For.CNVIII, foramen for the posterior branch of the vestibulo-acoustic nerve; For.CNX, foramen for vagus nerve; For.CNXII, foramina for hypoglossal nerve branches; Jg.For, jugular foramen; Lat.SMC, lateral semicircular canal; Oc.Cd, occipital condyle; Ot.Cr, otoccipital crest; Poc.Pr, paroccipital process; Pot.Sac, periotic (perilymphatic) sac; Post.SMC, posterior semicircular canal; V.FP.Cr.Inf, ventral foot process of the crista interfenestralis; Wv.Fc, Wever's facet. Scale = bar, 1 mm. Arrowhead points to the rostral end of the cranium

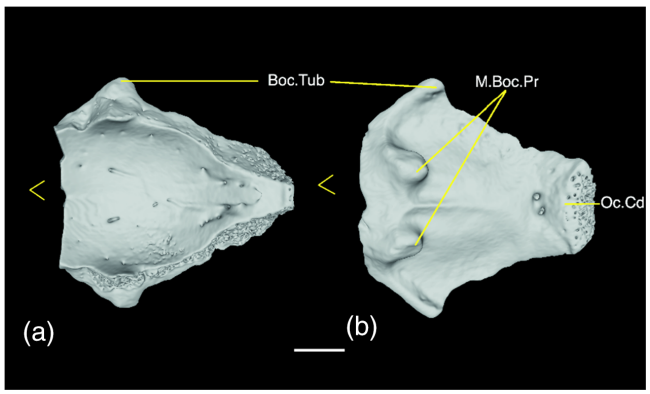

FIGURE 13 *Hypoptophis wilsonii* (RBINS-VER-REP 9712a), basioccipital. (a) Dorsal and (b) ventral views. Boc.Tub, basioccipital tubercle (spheno-occipital tubercle); M.Boc.Pr, medial basioccipital process; Oc.Cd, occipital condyle. Scale bar—1 mm. Arrowhead points to the rostral end of the cranium

Palatine

The palatine bears nine recurved teeth in all studied specimens. Palatine teeth are almost similar sized, the middle ones being only a little longer than the anterior and the posterior teeth (Figures 15a,b and S9). Lateral to the fourth to sixth teeth from the rostral end, the maxillary process juts out (Figures 15a,c,d and S9). The base of this process is pierced by a canal for the passage of the infraorbital division of the maxillary ramus of the trigeminal (CN V_2) nerve (Auen & Langebartel, 1977). Caudad to the maxillary process, the choanal process originates from the dorsal surface of the palatine. The choanal process in this species has a curious split structure (Figure 15a–d); it has a broad base and from there it rises first straight up, tapering as it goes, and then turns anteromedial. The next part of the choanal process, a slender semilunar ring of bone, is detached or "split" from the main body of the choanal process. This ring-like structure curves anteromedial and finally ends up turning posteroventral. Despite being proximal to the vomer, it does not make contact with that bone. The posterior end of the palatine has a well-developed pterygoid process which overlaps the dorsal surface of the proximal end of the pterygoid (Figure 15a–d). McDowell (1975) and Kluge (1993) termed it as a medial pterygoid process in pythons. Between the proximal end of the pterygoid process and the rearmost tooth, there is a notch with a posteriorly convex surface, which forms a saddle joint with the anterior end of the pterygoid.

Pterygoid

The pterygoid is the longest element of the palatomaxillary arch. It is a dagger-shaped bone bearing 10 to 13 small, recurved teeth which become gradually smaller posteriorly (Figures 16a,b and S9). The teeth are located along the medial edge of the anterior half of the pterygoid.

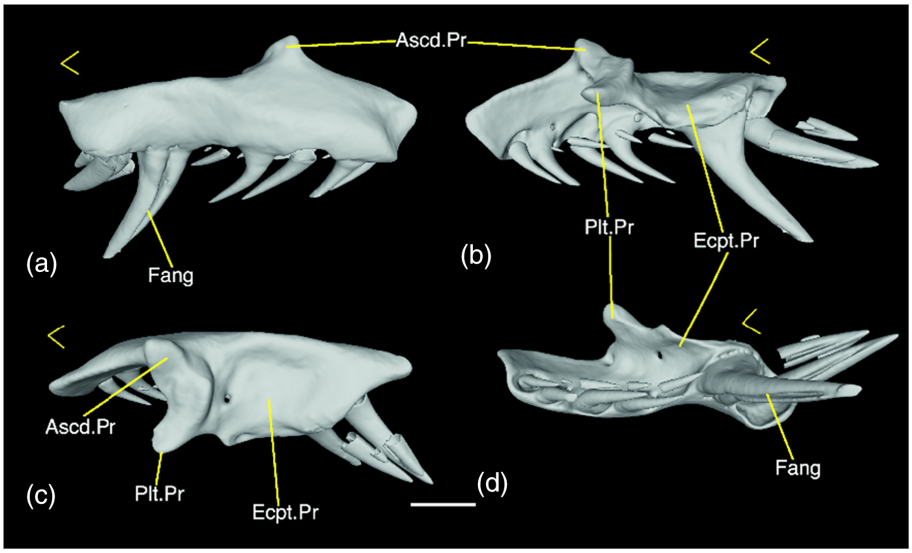

FIGURE 14 *Hypoptophis wilsonii* (RBINS-VER-REP 9712a), right maxilla. (a) Lateral, (b) medial, (c) dorsal, and (d) ventral views. Ascd.Pr, ascending process; Ecpt. Pr, ectopterygoid process; Fang, grooved fang; Plt.Pr, palatine process. Scale bar—1 mm. Arrowhead points to the rostral end of the cranium

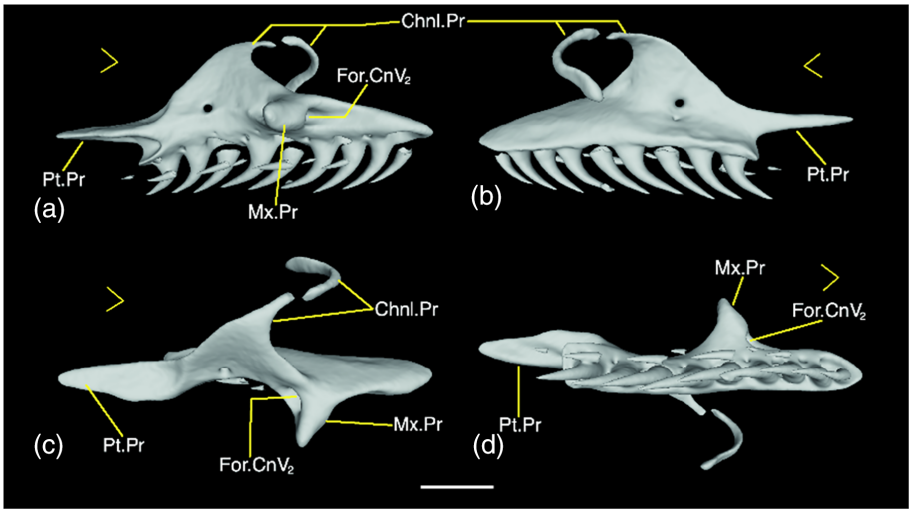

FIGURE 15 *Hypoptophis wilsonii* (RBINS-VER-REP 9712a), right palatine. (a) Lateral, (b) medial, (c) dorsal, and (d) ventral views. Chnl.Pr, choanal process; For.CNV$_2$, foramen for infraorbital division of trigeminal maxillary ramus; Mx.Pr, maxillary process; Pt.Pr, pterygoid process. Scale bar = 1 mm. Arrowhead points to the rostral end of the cranium

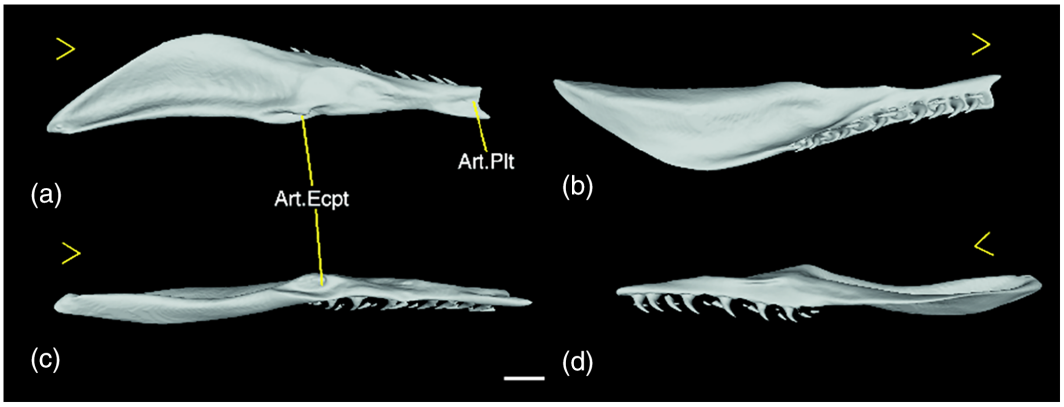

FIGURE 16 *Hypoptophis wilsonii* (RBINS-VER-REP 9712a), right pterygoid. (a) Dorsal, (b) ventral, (c) lateral, and (d) medial views. Art.Ecpt, articular surface for ectopterygoid; Art.Plt, articular surface for palatine. Scale bar = 1 mm. Arrowhead points to the rostral end of the cranium

The rostral end of the pterygoid is emarginated and meets the articular surface of the palatine in a saddle joint (Figure 16a,b). The dorsal surface of the pterygoid's anterior end has a small, elongated concavity (extending back up to the level of the fourth/fifth tooth from the proximal end), which is overlapped by the pterygoid process from the palatine (Figure 16a). Along the lateral side of the dorsal surface of the pterygoid's

posterior half (the quadrate ramus of the pterygoid), there is an extensive longitudinal concavity for the insertion of the M. protractor pterygoidei (Figure 16a). A longitudinal convexity along the ventral surface of the posterior half of the pterygoid corresponds to the dorsal concavity. Immediately rostrad to the aforementioned concave insertion site for the M. protractor pterygoidei, there is a small concave articulatory surface for the caudal end of the ectopterygoid (Figure 16a,c). Caudally, the pterygoid extends a little past the quadrate-mandible articulation to which it is proximate. The pterygoid on the right side of the head is broken in the male specimen.

Ectopterygoid

The ectopterygoid acts as a bridge between the pterygoid and the maxilla. Anteriorly, the ectopterygoid is emarginated and is produced into elongated anteromedial and short anterolateral lobes (Figure 17a,b; sensu McDowell, 1986). This part of the ectopterygoid partially overlaps the caudal end of the maxillary ectopterygoid process, with the anteromedial process following the medial edge of the maxillary ectopterygoid process. Posteriorly, the ectopterygoid tapers gradually to a point and articulates with the dorsolateral surface of the pterygoid (Figure 17b,c).

3.1.4 | Suspensorium and mandible

The mandible is attached to the braincase through the quadrate which, in turn, attaches to the supratemporal (Figure 1). The mandible has two major components—compound bone and dentary. The dentary is the sole dentigerous element of the lower jaw. The compound bone is a composite of prearticular, surangular, and articular. Medially, the mandible has two more small constituents, namely angular and splenial.

Supratemporal

Werneburg and Sánchez-Villagra (2015) suggested that the supratemporal might be the homolog of squamosal, while McDowell (2008) posited that this bone should be regarded as a tabular in diapsids, including snakes. Medially, the supratemporal articulates with the dorsolateral surface of the prootic. The anteriorly directed process articulating to the prootic (Figure 18a,b) was termed the anterodorsal process by McDowell (2008), who previously termed the same process as the parietotabular arch process (McDowell, 1987). At about the midpoint of the supratemporal, dorsal to the crista circumfenestralis dorsalis (to be more specific, lateral to the digitiform process of the otoccipital), there is a ventral expansion (Figure 18a,b) which was called the paroccipital process lobe and the anteroventral lobe by McDowell (1987) and McDowell (2008), respectively. Posterior to this anteroventral or paroccipital process lobe, the supratemporal starts to gradually taper and turns a little medial. The cephalic condyle of the quadrate articulates lateral to this part of the supratemporal. The caudal end of the supratemporal does not reach the end of the braincase.

Quadrate

The quadrate is short in this species, and its articulation with neither the supratemporal nor the compound bone goes past the caudal end of the braincase (Figure 1b). The medial surface of the cephalic condyle of the

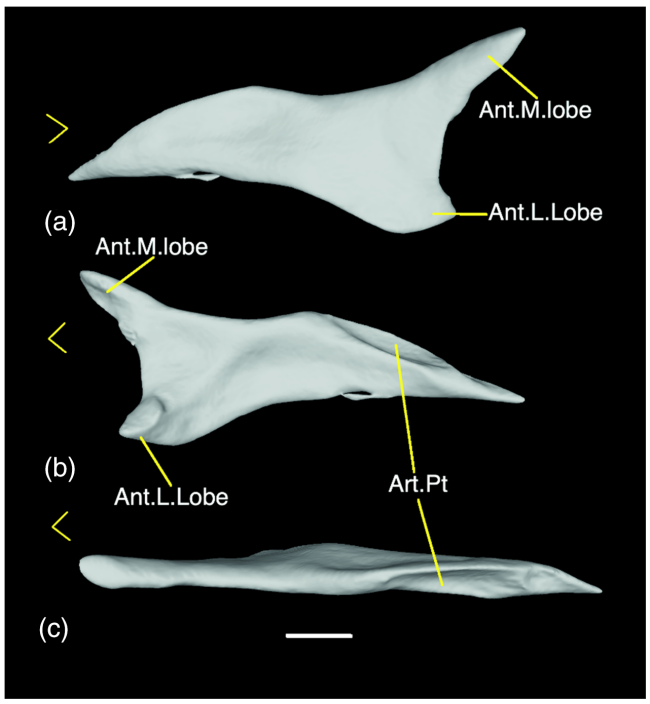

FIGURE 17 *Hypoptophis wilsonii* (RBINS-VER-REP 9712a), right ectopterygoid. (a) Dorsal, (b) ventral, and (c) lateral views. Ant.L.Lobe, anterolateral lobe; Ant.M.Lobe, anteromedial lobe; Art.Pt, articular surface for pterygoid. Scale bar—1 mm. Arrowhead points to the rostral end of the cranium

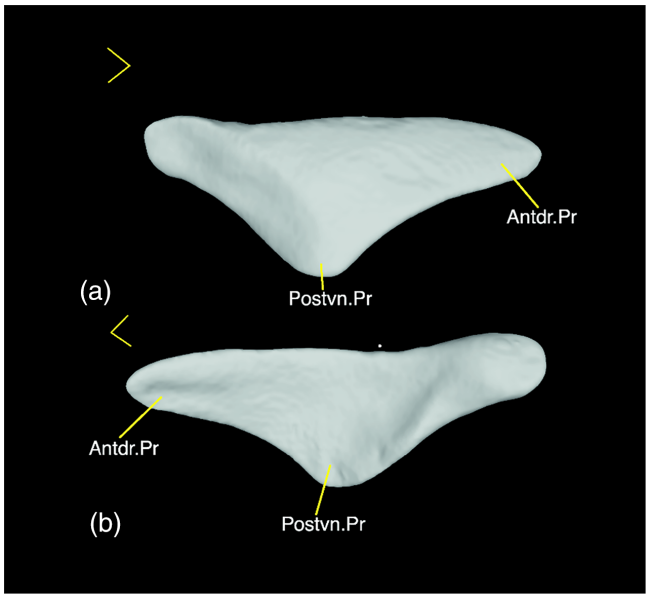

FIGURE 18 *Hypoptophis wilsonii* (RBINS-VER-REP 9712a), right supratemporal. (a) Lateral and (b) medial views. Antdr.Pr, anterodorsal process ("parietotabular arch" process); Postvn.Pr, posteroventral process ("Paroccipital process lobe"). Scale bar = 1 mm. Arrowhead points to the rostral end of the cranium

quadrate articulates with the supratemporal. The cephalic condyle is expanded, mainly in the anterior direction and lateromedially compressed, especially its dorsal and posterior aspects (Figure 19a,b). The quadrate tapers anteroposteriorly but thickens lateromedially toward the ventral end. Along the anterolateral surface of the quadrate shaft, there is an adductor ridge for the M. adductor mandibulae externus superficialis (Figure 19a; Das & Pramanick, 2019). The anterior surface of the bone is rather flat and probably serves as the site of origin of the M. adductor posterior (Das & Pramanick, 2019). Ventrally, the quadrate shaft expands lateromedially to form a trochlea (Figure 19a–d; "trochlea quadrati" of Szyndlar, 1984) which articulates with the compound bone in a saddle joint. Immediately dorsal to the quadrate trochlea, on both the anterior and posterior surface of the bone, and on the lateral surface of the cephalic condyle, there is a variable number of small foramina. On the medial surface of the quadrate shaft, there is a discoid stylohyal which protrudes slightly past the caudal edge of the quadrate (Figure 19b).

Compound bone

The constituents of the compound bone, namely the articular, the prearticular and the surangular, are completely fused as is typical for snakes. The articular has a deep articular surface resembling a saddle upon which the quadrate trochlea sits (Figure 20a–c). On the ventral surface of the articular, there is a short, indistinct, longitudinal ridge which is likely to serve as the insertion site of the M. pterygomandibularis accessorius (Figure 20d). Caudad to the articular surface for the quadrate trochlea is a retroarticular process, which is perforated by a chorda tympani (CN VII) foramen on its dorsomedial surface and another foramen on the lateral surface (which connects internally to the chorda tympany foramen; Figure 20b). The chorda tympani nerve foramen opens, after running rostrad, in the mandibular fossa. A deep mandibular or adductor fossa is walled laterally by surangular and medially by prearticular (Figure 20c). The prearticular crest is a little higher than the surangular crest. Anterior to the mandibular fossa, the compound bone has an alveolar canal, completely enclosed by the prearticular and surangular, through which the mandibular branch of the trigeminal (CN V_3) nerve (inferior alveolar nerve) runs rostrad (Auen & Langebartel, 1977). Just ahead of the mandibular fossa is a low but distinct dorsolateral (surangular) ridge, a pseudocoronoid process (sensu McDowell, 1968), which may serve as the site of insertion of the M. adductor mandibulae external medialis-profundus slip (Figure 20a,c). A branch off the inferior alveolar nerve emerges through a lateral foramen on surangular (Figure 20a). There are, however, two lateral surangular foramina in RBINS-VER-REP 9711. Rostral to the lateral surangular foramen, the compound bone gives rise to a dorsolateral tapering projection which fits into a notch (part of the alveolar nerve canal) between the posterior dorsal and ventral processes and the intermandibular septum of the dentary bone. Medially and ventrally, that is, on the prearticular side, the compound bone does not extend rostrally beyond the anterior end of the angular and is notched for the passage of the mylohyoid (CN V_3) nerve (McDowell, 2008; Figure 20b, d). The ventrolateral surface of the anterior end of the compound bone where the angular articulates is modified into an articular surface, that is, two narrow longitudinal strips of concavity alternating with two elongated ridges.

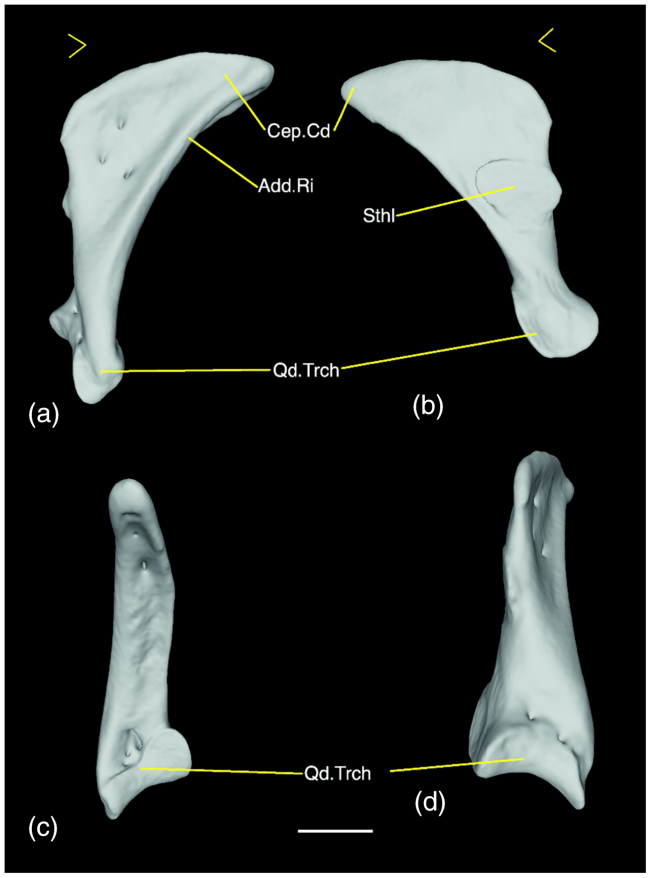

FIGURE 19 *Hypoptophis wilsonii* (RBINS-VER-REP 9712a), right quadrate. (a) Lateral, (b) Medial, (c) anterior, and (d) posterior views. Add.Ri, adductor ridge, Cep.Cd, cephalic condyle of quadrate; Sthl, stylohyal; Qd.Trch, quadrate trochlea. Scale bar—1 mm. Arrowhead points to the rostral end of the cranium

Dentary

The dentary is the dentigerous bone of the mandible, whose tapering and medially-turned anterior end does not reach past the rostral end of the maxilla in the articulated skull, thus resulting in a countersunk mouth. This bone bears 13 teeth in all the studied specimens except on the left dentary of RBINS-VER-REP 9712b, which bears 14 teeth. The dentary teeth become gradually smaller caudally (Figure 21a,b). *Hypoptophis* has well-developed posterior dorsal and posterior ventral processes on its dentary, with the former being only slightly longer than the latter (Figure 21a–c). The posterior ventral process has an articular surface along its medial ventral border for the splenial. An intramandibular septum separates the laterally and dorsally running alveolar nerve canal and the medial and relatively ventral Meckelian groove (Figure 21a,b). In RBINS-VER-REP 9211, a male, the alveolar canal in the articulated mandible exposes itself in the lateral view only slightly before running rostrad entirely internally through the dentary, and there is a mental foramen. In RBINS-VER-REP 9712a and 9712b—both females—the alveolar canal remains exposed in the

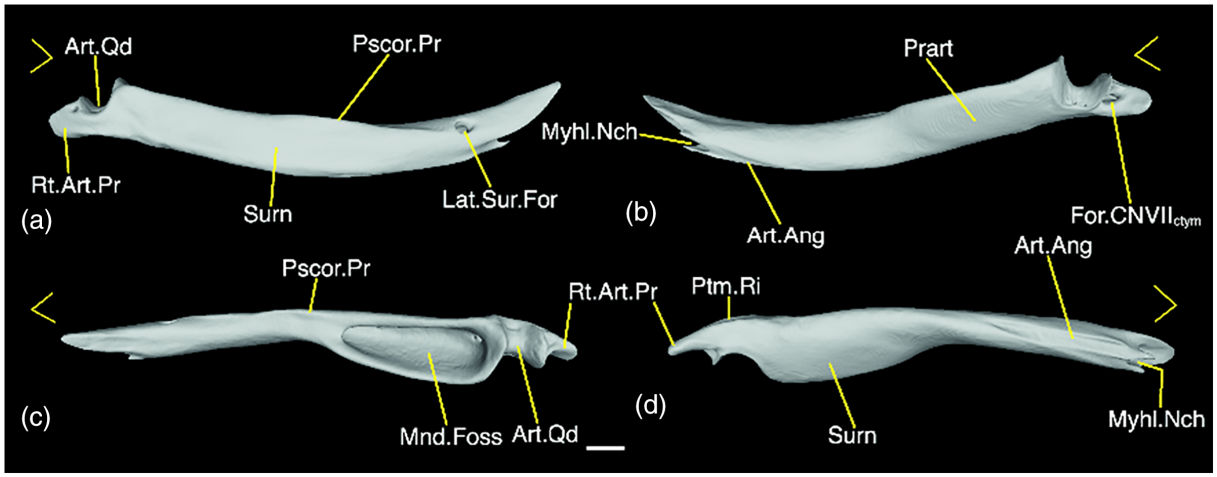

FIGURE 20 *Hypoptophis wilsonii* (RBINS-VER-REP 9712a), right compound bone. (a) Lateral, (b) medial, (c) dorsal, and (d) ventral views. Art.Ang, articular surface for angular; Art.Qd, articular surface for quadrate trochlea; For.CNVII$_{ctym}$, chorda tympani nerve foramen; Lat.Sur.For, lateral surangular foramen; Myhl.Nch, mylohyoid notch; Pscor.Pr, pseudocoronoid process; Prart, prearticular; Ptm.Ri, idge receiving the slip of M. pterygomandibularis accessorius; Rt.Art.Pr, retroarticular process; Surn, surangular. Scale bar = 1 mm. Arrowhead points to the rostral end of the cranium

FIGURE 21 *Hypoptophis wilsonii* (RBINS-VER-REP 9712a), right dentary. (a) Lateral, (b) medial, and (c) dorsal views. Alv.C, alveolar canal; Int.Mnd.Spt, intramandibular septum; Mcl.Gr, meckelian groove; Mnd.Foss, mandibular fossa; Post.Dr.Pr, posterior dorsal process; Post.Ven.Pr, posterior ventral process. Scale bar—1 mm. Arrowhead points to the rostral end of the cranium

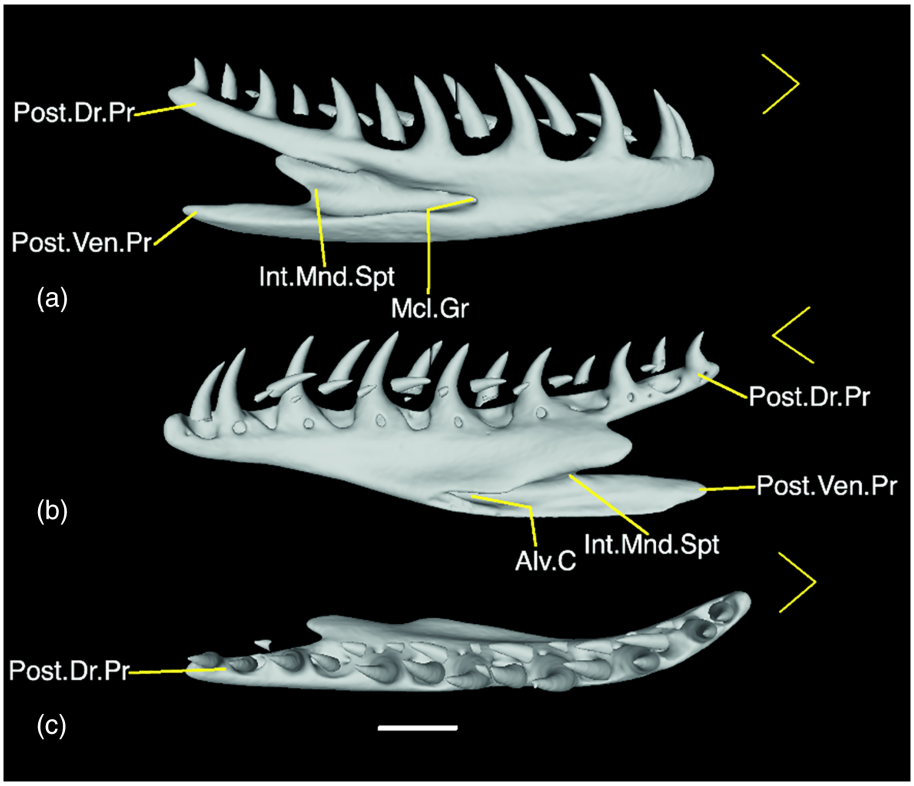

lateral view for a longer stretch and thus fully incorporates the mental foramen into it. Like the alveolar nerve canal, the Meckelian groove also becomes completely enclosed inside the dentary at a point where the anterior tip of the splenial lies in the articulated mandible.

Angular

This is an elongated triangular splint of bone attached to the ventro-medial surface of the compound bone (Figure 22b,c), acting as a medial wall for the mylohyoid notch in the latter. The caudal end is pointed, and the anterior end rises up and articulates with the splenial, medial to the posterior ventral process of the dentary (Figure 1a). A small posterior mylohyoid foramen perforates the angular near its anterior end (Figure 22b,c; absent in the left angular of RBINS-VER-REP 9712a and 9711, with the myolohyoid nerve branchlet possibly emerging through a slight recess between the angular and splenial in such cases).

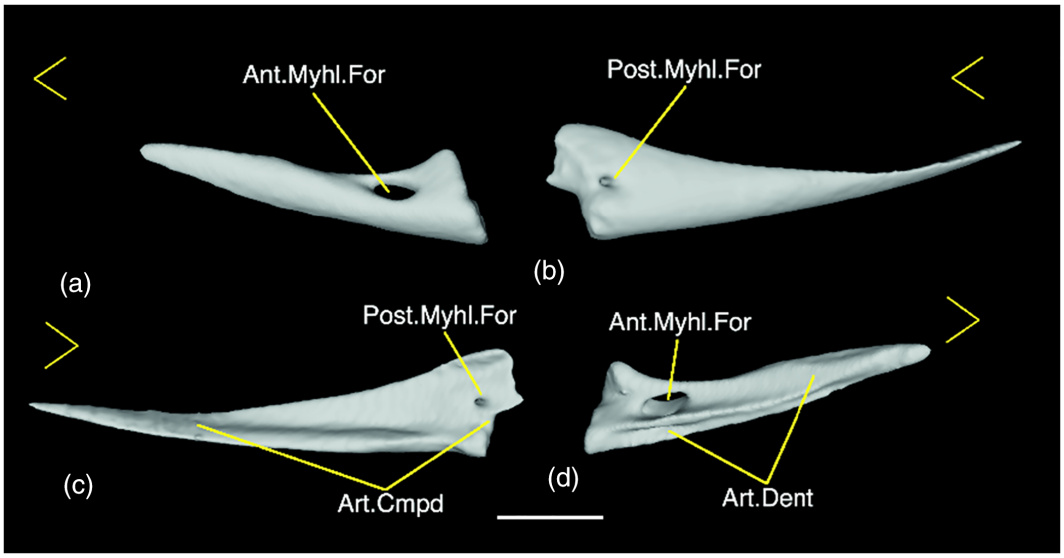

FIGURE 22 *Hypoptophis wilsonii* (RBINS-VER-REP 9712a), right angular and splenial angular. (b) Lateral and (c) medial views, splenial—(a) lateral and (d) medial views. Ant.Myhl.For, anterior mylohyoid foramen; Art.Cmpd, articular surface for compound bone; Art.Dent, articular surface for dentary; Post.Myhl.For, posterior mylohyoid foramen. Scale bar = 1 mm. Arrowhead points to the rostral end of the cranium

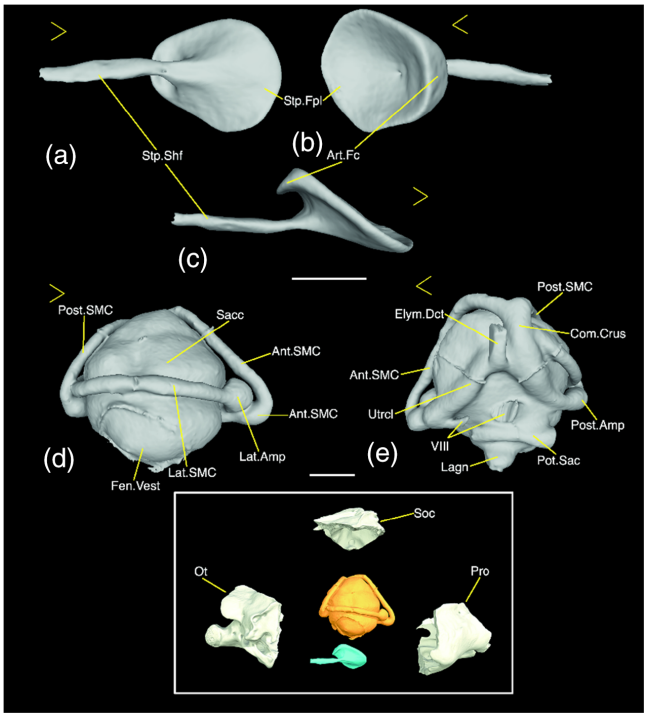

FIGURE 23 *Hypoptophis wilsonii* (RBINS-VER-REP 9712a), middle ear bone and inner ear endocast, from the right side, stapes—(a) lateral, (b) posteromedial, and (c) dorsal views, inner ear endocast—(d) lateral and (e) medial views; inset—middle and inner ear with respect to the otic capsule bones. Ant.Amp, anterior ampulla; Ant.SMC, anterior semicircular canal; Art.Fc, articular facet; Com.Crus, common crus; Elym.Dct, endolymphatic duct; Fen.Vest, fenestra vestibuli; Lagn, lagena; Lat.Amp, lateral ampulla; Lat.SMC, lateral semicircular canal; Post.amp, Posterior ampulla; Post.SMC, posterior semicircular canal; Pot.Sac, periotic (perilymphatic) sac; Sacc, sacculus; Stp.Fpl, stapedial footplate; Stp.Shf, stapedial shaft; Utrcl, utriculus; VIII, vestibulo-acoustic nerve. Scale bars = 1 mm. Arrowhead points to the rostral end of the cranium

Splenial

This is another elongated bone, although it is shorter than the angular. The splenial articulates laterally with the posterior ventral process of the dentary, ventromedial to the Meckelian groove, and posteriorly with the angular. The anterior mylohyoid foramen is distinctly larger than its posterior counterpart piercing

the angular. It perforates the splenial close to its caudal end (Figure 22a,d). The dorsal margin of the anterior mylohyoid foramen is incomplete in RBINS-VER-REP 9711.

3.1.5 | Middle and inner ear

The stapes of the middle ear is a splanchnocranial bone. The otic capsule bones, namely prootic, supraoccipital and otoccipital enclose the structure of the inner ear. In the following description, those structures are described by alluding to the bones housing them so that the description facilitates interpretation of the internal surfaces of the otic capsule bones.

Stapes

The ovoid, medially concave stapedial footplate is large and forms an articular facet along its posterior periphery which abuts the Wever's facet (Figure 23a–c). The slender stapedial shaft is caudally slanted at a 45° angle relative to the stapedial footplate (Figure 23c).

Inner ear endocast

The laterally compressed, spherical sacculus is well-developed and much bigger than the lagena (Figure 23d), a feature observed in many fossorial taxa (Palci et al., 2017; Yi & Norell, 2015). The fenestra vestibuli is large, and the semicircular canals are rather narrow. The lateral (horizontal) semicircular canal runs through the dorsolateral wall of the prootic (Figure 23d), precisely medial to the site of attachment of the supratemporal, and enters the otoccipital dorsal to fenestra vestibuli. Moving caudad, the lateral semicircular canal passes around the sacculus, briefly contacting the posterior semicircular canal in the process and after taking the turn, runs medio-dorsad along the median wall of the otoccipital before joining the common crus (Figure 23e) on the median flange of the supraoccipital. The anterior semicircular canal takes a dorsomedial course from the anterior ampulla through the prootic and enters the supraoccipital, where it meets the posterior semicircular canal (Figure 23d+e). The posterior semicircular canal courses ventrolateral through the supraoccipital to enter the otoccipital (Figure 23d+e). Then it bends around the sacculus to reach the

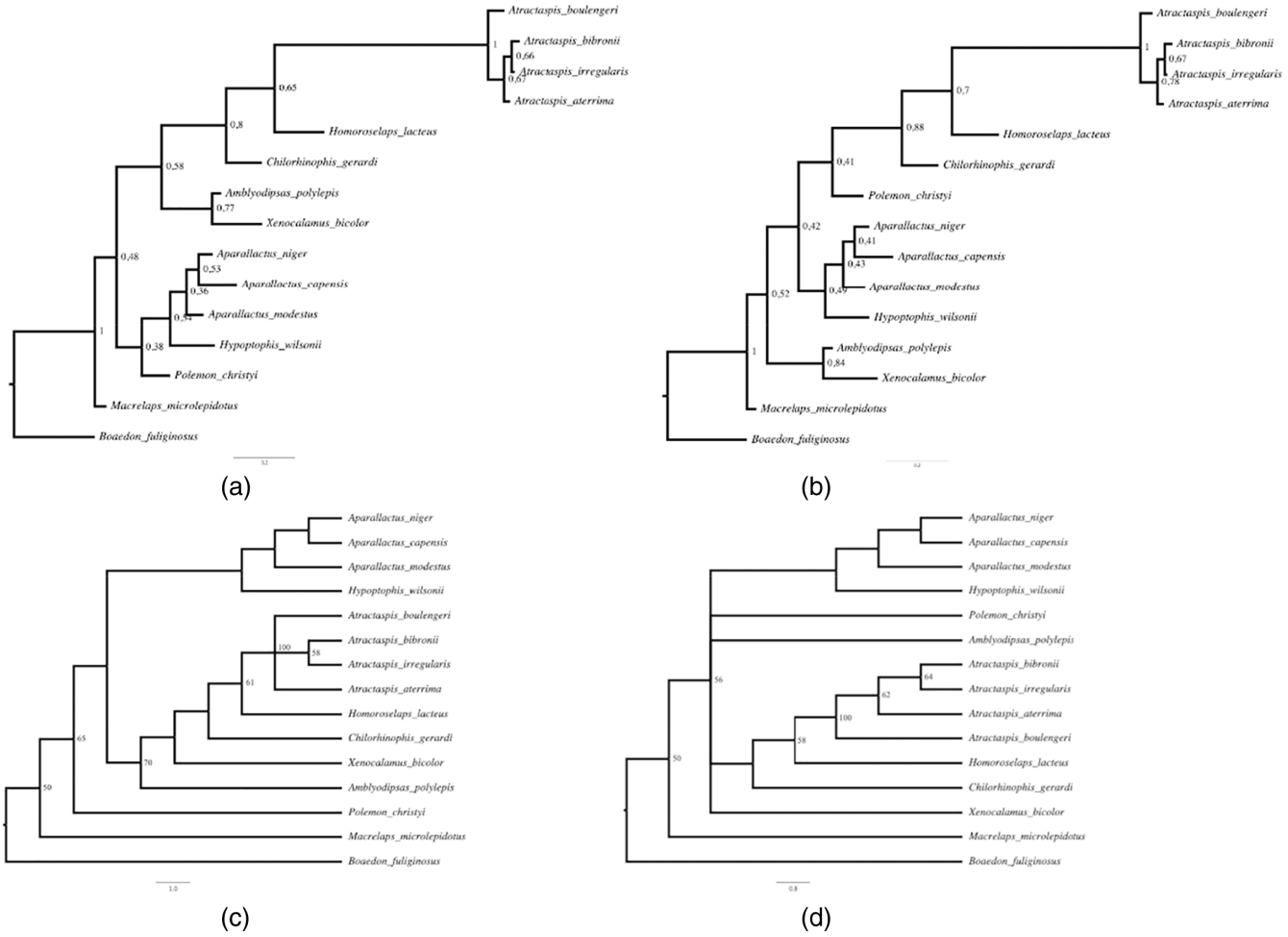

FIGURE 24 Bayesian Inference phylogenies, based on (a) ordered and (b) unordered data matrices; strict consensus of maximum parsimony phylogenies, based on (c) ordered and (d) unordered data matrices. The numbers beside the nodes represent posterior probabilities in (a) and (b), and bootstrap values in (c) and (d)

posterior ampulla medial to the sacculus, which eventually leads to the common crus.

3.2 | Phylogeny

The analyses with ordered and unordered character matrices converged in 1,520,000 and 1,310,000 generations, respectively. Potential Scale Reduction Factor values were ~1. Analysis of runs with Tracer 1.7 confirmed the convergence.

The monophyly of Atractaspididae was strongly supported with a posterior probability (PP hereafter) of one. *Macrelaps* is recovered as the basal-most taxon in both analyses (Figure 24). Atractaspidinae formed a monophyletic subclade in both trees, although with low to moderate PP. However, unlike molecular phylogenies (e.g., Portillo et al., 2018, 2019), Aparallactinae was not recovered as monophyletic with respect to Atractaspidinae. The PPs of the deeper splits were low to moderate (Figure 24). All genera for which more than one species was available, namely *Aparallactus* and *Atractaspis*, were monophyletic (Figure 24). *Hypoptophis* was found to be the sister taxon to *Aparallactus* in both analyses, albeit with poor support (PP 0.54 and 0.49 for the ordered and unordered character matrix, respectively). There were some topological differences between the phylogenies inferred from the analyses on the ordered and unordered matrices (Figure 24).

Maximum Parsimony analyses on both the ordered and unordered data matrices returned the two most parsimonious trees, with some topological differences (Figures 24c,d and S5A–C and S6A–C). In total, 52 character statements were Parsimony-informative. Aparallactinae was monophyletic, although Atractaspidinae was invariably found to be monophyletic. In the four most parsimonious trees, *Hypoptophis* was recovered as a sister taxon to *Aparallactus*

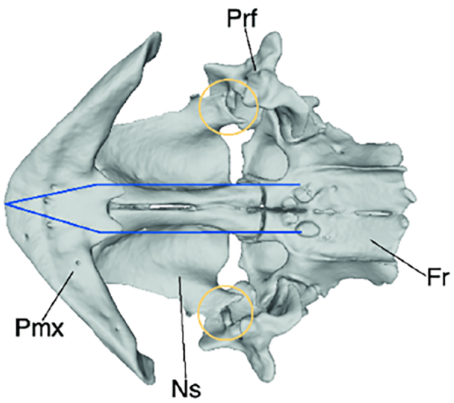

FIGURE 25 *Hypoptophis wilsonii* (RBINS-VER-REP 9712a), ventral view of the premaxilla, nasals, prefrontals, and the frontal, showing the "central rod" (indicated with blue lines) —The primary loading stress-bearing axis consisting of the premaxilla, the medial vertical laminae of the nasals and the subolfactory processes, and the medial flanges of the frontals (as well as the "outer shell," indicated with ochre circles—a contact between the posteroventral process from the nasal horizontal laminae and the prefrontals

(Figures S5A–C and S6A–C). Bootstrap support for all branches was mostly low. Consistency, retention, and rescaled consistency indices, along with tree length are given in Data S1.

4 | DISCUSSION

4.1 | Fossorial adaptations

Snout complex bones usually undergo adaptation for life beneath the surface, be it in highly fossorial snakes in which the entire cranium is adapted for a fossorial existence (viz. uropeltids [Comeaux et al., 2010; Olori & Bell, 2012]), or in semifossorial snakes with less extensive skull specializations for a subterranean mode of life (e.g., some colubrids, such as *Argyrogena* [Das et al., 2019]), although the elapid *Aspidelaps* is a known deviation from this norm (Deufel, 2017). Snout complex bones of the fossorial and semifossorial snakes also frequently have increased points or surfaces of contact among themselves and with other cranial elements (Savitzky, 1983). In *Hypoptophis*, the nasals diverge anteriorly, with the vertical laminae forming an articular surface upon which the triangular ascending process of the premaxilla rests. This state is seen in other aparallactines genera as well, although the degree to which the ascending process separates the rostral ends of the nasal differs. In *Amblyodipsas* and especially in *Xenocalamus* (also in *Macrelaps*, although to a lesser extent), an elongated premaxillary ascending process wedges amidst the vertical laminae of the nasals for a considerable length, thus resembling the configuration of uropeltids. However, the premaxillary process running caudad between the nasals in most basal alethinophidians, including uropeltids, is probably a nasal process and therefore unlikely to be homologous with the similar structure in the aparallactines (Cundall & Irish, 2008). The transverse processes of the premaxilla of *Hypoptophis* appear to stay in a syndesmotic contact with the maxilla's anterior end, and both these elements have modified surfaces to facilitate the loose contact, although there is no "schizarthrotic" articulation between the premaxilla and maxilla, as in many uropeltids (Olori & Bell, 2012; Rieppel & Zaher, 2002). Some other aparallactines have a similar premaxilla–maxilla contact, mediated by somewhat similar modifications on the contact surfaces of both bones. The prosymnid *Prosymna lineata* has a similar contact between these two elements (Figure 5 of Heinicke et al., 2020). Among the basal fossorial alethinophidians, various forms of contact between the transverse process of the premaxilla and maxilla have also been noted (Comeaux et al., 2010; Frazzetta, 1999; Olori & Bell, 2012; Rieppel & Maisano, 2007; Rieppel & Zaher, 2002).

The nasal horizontal lamina establishes contact with the prefrontal in *Hypoptophis*. The nasal–prefrontal articulation resembling that of *Hypoptophis* is observed in *Aparallactus niger* among the confamilial taxa. Savitzky (1983) reported and illustrated the nasal–prefrontal contact, although formed in a somewhat different way, in the fossorial psammophiid *Rhamphiophis* and colubrid *Tantilla*. Various forms of connection between these two bones are found in "scolecophidians" (Chretien et al., 2019; Cundall & Irish, 2008) and in fossorial basal

alethinophidians (Cundall & Rossman, 1993; Comeaux et al., 2010; Olori & Bell, 2012; Frazzetta, 1999; Cundall & Irish, 2008; present study). Although pythons and boas also have the nasal in contact with the prefrontal, this contact is mediated by a well-developed dorsal lappet from the nasal (Cundall & Irish, 2008; Frazzetta, 1966), which does not appear to be adapted for burrowing. Nasal–prefrontal contact is noted in the stem snake *Dinilysia patagonica* too (Zaher & Scanferla, 2012), which might have a semifossorial-semiaquatic lifestyle like some homalopsids (Palci et al., 2017). The nasofrontal joint in *Hypoptophis* is formed by extensive contact between the nasal and the frontal medial flanges, as is typical of fossorial basal alethinophidians (e.g., xenopeltids, loxocemids [Rieppel, 2007]), fossorial colubrids (Das et al., 2019; Rieppel, 2007) and most aparallactines and atractaspidines (Strong et al., 2020; present study).

Bourgeois (1968) inferred that aparallactines and atractaspidines are closely related to each other based on her observation of the way the maxilla articulates with the prefrontal by means of an ascending process ("processus vertical" of Bourgeois, 1968) in both groups (her Aparallactinae)). Nevertheless, this association and whether it could be indicative of a causal relation with any particular ecological or functional trait behind the development of such a process has never been adequately discussed in the broader context of different snake lineages having this character state. A distinct ascending process partaking in maxilla-prefrontal articulation is present in stem snakes *Parviraptor*, *Diablophis*, *Portugalophis* (Caldwell et al., 2015), *Dinilysia* (Zaher & Scanferla, 2012), *Najash* (Garberoglio et al., 2019), *Coniophis* (Longrich et al., 2012), extinct madtsoiid *Sanajeh*, *Wonambi*, and *Yurlunggur* (Scanlon, 2005, 2006; Wilson et al., 2010), extinct simoliophiid *Pachyrhachis* (figure 2f,h of Caldwell & Lee, 1997), and Aniliidae, Cylindrophiidae and Uropeltidae (Cundall & Irish, 2008; Olori & Bell, 2012) among non-caenophidians. The ascending process of *Aparallactus*, *Hypoptophis*, *Macrelaps* and to some extent, *Amblyodipsas* is similar to that of uropeltids. Interestingly, all these extant taxa are fossorial, while among the extinct ones, at least *Dinilysia*, *Coniophis*, and *Yurlunggur* (a madtsoiid) had some traits indicating a semifossorial lifestyle (Longrich et al., 2012; Palci et al., 2017, 2018). The same might (or might not) apply to *Najash* as well (Apesteguía & Zaher, 2006). The ascending process facilitates a robust articulation with the prefrontal, and hence reinforces the contact between maxilla and prefrontal, consistent with the tendency toward achieving a higher amount of compactness in fossorial snake crania. In some taxa, namely uropeltids, *Hypoptophis* and some *Aparallactus* with a prominent maxillary ascending process, there is contact between maxilla and premaxilla. It also appears likely that the lodging of the ascending process into the prefrontal ventrum resists any posterior displacement of the maxilla during pushing in soil with the snout tip. It is worth noting here that diapsid, including lepidosaurian, the maxillae frequently have a well-developed facial or ascending process which variably contacts the lacrimal, prefrontal, or both (e.g., Chapelle & Choiniere, 2018; Evans, 2008; Rauhut et al., 2010); in these, the maxillae are firmly associated to the skull.

Another feature of the maxilla of *Hypoptophis* that warrants discussion is the apposition of the palatine process and the ectopterygoid process. In most colubroids having both processes, the medially expanded ectopterygoid process is located farther back, separated from the palatine process (another medial expansion) by a narrower stretch of maxillary shaft (e.g., the maxilla of the colubrid *Hierophis* described by Racca et al., 2020). In Aparallactines, barring the centipede eating *Aparallactus* spp., the ectopterygoid process is separated from the palatine process merely by a notch (Figure S3). Maxillary fangs of rear-fanged snakes lie below the ectopterygoid process and thus, the shortening or loss of the maxillary shaft intervening between the palatine and ectopterygoid processes has the effect of bringing the fang closer to the rostral end of the gape. Among the examined aparallactines with shortened maxilla, *Amblyodipsas polylepis*, *Chilorhinophis gerardi* and *Xenocalamus bicolor* are known to prey principally on amphisbaenians, fossorial skinks, and snakes (Conradie & Pinto, 2021; Douglas, 1982; Marais, 2004; Shine et al., 2006; Spawls et al., 2018). It is noteworthy that we observed a *Zygaspis quadrifrons*, an amphisbaenid, inside the male *Hypoptophis* (RBINS-VER-REP 9711). This is the first record of a prey item of this species, and confirms Broadley's (1960) assumption on the diet of this snake (Figure S4). *Macrelaps microlepidotus* is a predator of frogs, lizards, small mammals, and snakes (Marais, 2004; Shine et al., 2006). In all these taxa, the ectopterygoid process is located directly behind the palatine process, thus bringing the fang below the orbit. *Polemon christyi* is known to feed chiefly on snakes, which holds true for other congeners as well (Shine et al., 2006). In this species, however, the fang is more rostrally placed, being located below the prefrontal, perhaps helping it to secure a grip on wriggling, scaly snake prey. Portillo et al. (2019) opined that a more rostrally positioned fang can help in restraining and envenomating strong squamate prey and can make maneuvering prey easier within narrow burrows. A complete confluence of the palatine and ectopterygoid processes, thus bringing the fang farther forward and almost below the maxillary ascending process (and thus, right below the articulation of this process with the prefrontal), coupled with a reduction of the anterior tooth-bearing part of the maxilla to a vestigial protuberance would produce the morphology seen in *Atractaspis* and *Homoroselaps*. We postulate that the maxilla of atractaspidines mostly represents the ectopterygoid process of most rear-fanged aparallactines (including rear-fanged colubroids). The way a medial process on the rostral end of the ectopterygoid—likely a homolog of the ectopterygoid anteromedial process—establishes contact with the medial aspect of the maxilla in *Atractaspis* adds further credence to our proposed homology. The anteromedial process from the ectopterygoid contacts the median margin of the maxillary ectopterygoid process in all the studied aparallactines. In *Atractaspis*, the lateral and ventral laminae of the prefrontal have become anteromedially twisted (Figure S2). Consequentially, the prefrontal lateral foot process and the ventral concavity accommodating the maxillary ascending process are more transversely positioned in this genus. These peculiarities of the prefrontal of *Atractaspis* have implications for identifying the actual homolog of the ascending process. The maxilla of *Atractaspis* has three dorsally directed protuberances (Strong et al., 2020). Among these, the anterior one, which is located medial to the lateral foot process in the articulated skull

(equivalent to being rostrad to the lateral foot process in the aparallactine prefrontal, which is not medially twisted) abuts the anteroventral aspect of the prefrontal's ventral concavity. This is the actual maxillary ascending process (Figure S3), not the posterolateral protuberance as indicated by Bourgeois (1968; see her figure 115). In keeping with the medially twisted prefrontal, the ascending process too has turned medial, and therefore appears anteroposteriorly compressed rather than lateromedially compressed as in most aparallactines. Finally, a homology between the aparallactines rear fang and the *Atractaspis* front fang corroborates and adds to the finding of Vonk et al. (2008) that the front fang in elapids and viperids actually represents the embryonic rear fang, which gets positioned anteriorly by developmental allometry. It is interesting to note that in typhlopids, the maxilla is transversely oriented and mobile (Cundall & Irish, 2008; Kley, 2001). Despite being designed to function differently, a medially twisted or transverse maxilla compensates for the difficulty of widely opening the mouth in a narrow burrow with a laterally swinging (in *Atractaspis* spp.) or raking (in typhlopids [Kley, 2001]) motion during subduing and/or ingesting prey.

Interestingly, *Hypoptophis* and many other aparallactines (but not atractaspidines) possess a split choanal process. A split choanal process with a free-floating slender part is also known from *Eryx*, a burrowing sand boa (figure 2.57 in Cundall & Irish, 2008; present study) although in that genus the base of the choanal process is only faintly developed. It seems likely that in these taxa, the choanal process develops from two ossification centers which fail to fuse at a later developmental stage. While this unusual character is seemingly rare even in fossorial taxa, its occurrence in distantly related burrowers like *Eryx* sand boas and aparallactines may indicate some relation with burrowing; confirming this requires functional morphological work.

Discussion on adaptations of the frontal bone for a burrowing mode of life often stresses upon the medial and the subolfactory/lateral frontal pillars (which fuse to form a single monolithic structure in caenophidians) and the robustness of the nasofrontal joint (e.g., Cundall & Rossman, 1993; Savitzky, 1983). In *Hypoptophis*, this character shows the typical state observed in connection with fossoriality, as discussed above. The dorsolateral surfaces of the frontals are modified into articulatory facets for the parietal supraorbital processes. This also contributes to an increased consolidation of the braincase and circumorbital elements.

The supraorbital process from the parietal, as observed in *Hypoptophis*, is another trait associated with fossorial or semifossorial habits. This anterolateral projection from the parietal, embracing the frontals tightly from both sides, is present in fossorial basal alethinophidians and many colubroids, including aparallactines (Cundall & Irish, 2008; Olori & Bell, 2012; Palci et al., 2018).

Fossorial snake taxa often tend to have fused brain case elements; the uropeltids furnish a classic example (Cundall & Irish, 2008; Olori & Bell, 2012). In uropeltids, all the chondrocranial elements fuse to form a single spheno-occipital complex (Olori & Bell, 2012). Fusion to a similar degree has taken place in aparallactine *Chilorhinophis* and *Xenocalamus bicolor* (whose skull superficially resembles that of uropeltids; the chondrocranial elements in the cranium of *X. mechowi* do not fuse together [Bourgeois, 1968]). We observed incomplete fusion between the prootic, the otoccipital, and the supraoccipital in one *Polemon christyi* skull (CAS-HERP 147905), but not in another (RMCA-VERT-R. 14373). The one *Hypoptophis* specimen (RBINS-VER-REP 9711) with its parabasisphenoid and basioccipital almost completely fused may be indicative of a tendency toward fusion. A tendency toward fusion is seen in burrowing prosymnids as well (Heinicke et al., 2020).

While *Hypoptophis* has a distinct dorsum sellae, this is not developed in *Amblyodipsas*, *Aparallactus capensis*, *Chilorhinophis*, *Polemon*, and *Xenocalamus*. The atractaspidine basisphenoid is also devoid of a dorsum sellae (Strong et al., 2020; present study), as well as Scolecophidia (Chretien et al., 2019; Rieppel et al., 2009) and some fossorial basal alethninophidians (Olori & Bell, 2012; Rieppel, 1979; Rieppel & Maisano, 2007). Nevertheless, it should be noted that this character can be somewhat variable (Sheverdyukova & Kovtun, 2020; Strong et al., 2020) and not all burrowers lack a dorsum sellae.

None of the aparallactines show the marked modification of the mandible seen in *Atractaspis* and scolecophidians, produced by paedomorphosis (Kley, 2006; Strong et al., 2020). However, in *Xenocalamus*, the anterior end of the dentary is distant from the snout tip, thus producing a strongly subterminal mouth. Besides the snout and chondrocranial braincase, this is another conspicuous parallel of uropeltid morphology in *Xenocalamus*. *Amblyodipsas* and *Hypoptophis* also have a distinctly subterminal mouth, but the distance between the anterior tips of the premaxilla and dentary are much less than that seen in *Xenocalamus*. A subterminal, countersunk lower jaw is a common fossorial adaptation in snakes (Lillywhite, 2014). Although it cannot be definitively associated with burrowing, it is nevertheless of interest to note that a number of aparallactine species are characterized by the presence of a prominent "pseudocoronoid" or coronoid process. Among aparallactines, *Polemon* and *Chilorhinophis* compound bones develop a prominent pseudocoronoid process, but only in the latter does this process or ridge become nearly as prominent as that in the atractaspidine *Homoroselaps*. In other aparallactines, except *Aparallactus capensis* and *Xenocalamus bicolor* which both lack it, the pseudocoronoid process is merely a ridge. Although *Atractaspis* spp. do not usually possess this process (Strong et al., 2020; present study), we observed a weak coronoid process in *A. aterrima*, hence the presence of this process might be the ancestral state for Atractaspididae. The coronoid process, however, is poorly developed or completely lost in some aparallactines and most *Atractaspis* spp. (likely because of paedomorphosis in this particular genus). A coronoid process is present in many basal alethinophidian clades (Cundall & Irish, 2008).

Recently, the ophidian inner ear has garnered attention from anatomists (Olori, 2010; Palci et al., 2017, 2018; Yi & Norell, 2015), especially for the purpose of deducing the palaeoecology of basal, extinct lineages of snakes (e.g., Yi & Norell, 2015 and Palci et al., 2017, for *Dinilysia patagonica*). The inner ear of *Hypoptophis* is characterized by a large sacculus which is typically observed among burrowing snakes (Yi & Norell, 2015). Although there are exceptions

to this norm (Palci et al., 2018), observing it in *Hypoptophis* is fully consistent with its fossorial habits.

Hypoptophis wilsonii is considered to be a fossorial species (Broadley, 1960); since it has a wedge-like snout, it has been speculated that this snake burrows actively (Chippaux & Jackson, 2019). Our observations on the cranial osteology of this species appear to support the viewpoint that it is likely capable of digging. One of the primary cranial structural themes for burrowing is the "outer shell design" (Cundall & Rossman, 1993), exemplified by typhlopoid skulls. In such crania, the premaxilla, the nasals, and the prefrontals form a load-bearing encasing that meets the frontal, which lacks the medial flanges and to which the load is eventually transmitted dorsally and laterally. The other major structural design used for digging has been termed as the "central rod design" (Cundall & Rossman, 1993) where the load is borne principally by the premaxilla, vertical laminae of the nasals and medial flanges of the frontals. The archetypal central rod design can be seen in the snout bones and the prokinetic joint of uropeltids, as well as several other fossorial alethinophidians (Cundall & Rossman, 1993; Rieppel, 2007). A functional analogue of the alethinophidian central rod design in the anomalepidids, whose frontal is devoid of medial flanges, is achieved via a ventral contact between the nasal medial vertical lamina and the subolfactory process of the frontal (Rieppel et al., 2009). In leptotyphlopids, the nasals and prefrontals usually establish a dorsal and lateral contact with the dorsal horizontal and orbital laminae of the frontals, respectively, while the septomaxillae contacts the frontal subolfactory process ventrally (Koch et al., 2021; Martins et al., 2021; Rieppel et al., 2009). Hence, leptotyphlopid crania incorporate features from both the outer shell and the central rod designs to transmit the loading stress (Rieppel et al., 2009). Anomochilids furnish a classic example of incorporating features from both the paradigmatic alethinophidian central rod (i.e., mediated by nasal medial vertical lamina and medial frontal flanges) and outer shell designs (Cundall & Rossman, 1993; Rieppel & Maisano, 2007). A contact between the nasals and the prefrontals in *Aparallactus* has led Rieppel (2007) and Strong et al. (2020) to regard it as having elements of outer shell designs besides the central rod design typical of fossorial colubroids. The nasal-prefrontal contact is present in *Hypoptophis* as well, and therefore it too can be considered to have elements from the outer shell design (Figure 25). However, the principal load bearing axis, provided it burrows itself, is located along the premaxilla, nasal medial vertical lamina, and the medial frontal flange, as can be judged from the robustness of these structures themselves and of the articulations between them (Figure 25). Therefore, *Hypoptophis* appears to predominantly employ the central rod design to transmit the loading stress rearward. Overall, the shape of the premaxilla and its contacts with both the nasals and the maxilla, well-developed nasofrontal articulation and nasal-prefrontal contact suggests that *Hypoptophis* is able to burrow at least through loose substrate. In a recent study by Herrel et al. (2021), it has been demonstrated that scolecophidians mainly use anteriorly directed force during burrowing. Observations of live specimens of *Hypoptophis* are needed to validate the hypothesis that it is an active burrower, and if so, to study the functional morphological aspects of digging.

4.2 | Implications for the burrowing origin hypothesis

Based on the discussion presented above, most of the cranial osteological features of *Hypoptophis* and other aparallactines that can be associated with a fossorial lifestyle (including feeding habits) show homoplasious similarity to the cranial features of basal fossorial/semi-fossorial snakes. These putative adaptations for underground life are present in a number of basal snakes, including some of the earliest known species, but are lost in many afterward (e.g., in surface dwellers, arboreal species) and emerged again in many lineages (including several relatively unrelated groups of caenophidians). This pattern implies that these homoplasies can be reversals to the ancestral state (Wake et al., 2011). At the genetic level, these are possible cases of deep homology (Shubin et al., 2009; Wake et al., 2011), likely to have resulted from regulatory genetic element-mediated changes in gene expression (and therefore, developmental) patterns, which themselves are triggered by selection pressures associated with a subterranean lifestyle. However, it is interesting to note that apomorphic osteological features found only in lineages highly specialized for fossorial life do not show multiple gains-and-losses in different distantly related lineages. The peculiar palatomaxillary arch and mandible of scolecophidians, "schizarthrotic" premaxillary-maxillary suture of uropeltids, the unusual and the laterally swiveling maxilla of *Atractaspis* are examples of such anatomical specializations. Therefore, we concur with Caldwell (2020) that autapomorphic traits seen in obligate fossorial snakes are less likely to reverse. Hence, the chances of "stem snake" morphology, which are closely approached by scolecophidians as suggested by Da Silva et al. (2018), appear less probable. In fact, the choice of the phylogeny of Da Silva et al. (2018), which has scolecophidians as the basal-most snakes, might have led to this conclusion; none of the recent snake phylogenies of extant and extinct taxa (e.g., Gauthier et al. (2012); Longrich et al., 2012; Zaher & Scanferla, 2012; Caldwell et al., 2015; Hsiang et al., 2015; Martill et al., 2015; Garberoglio et al., 2019; Fachini et al., 2020) recovered scolecophidians as the most basal snakes. Strikingly, a recent reconstruction of the probable ancestral snake skull by Watanabe et al. (2019) resembles that of *Aparallactus*. Recent discoveries of snake fossils and palaeoecological inferences indicate that snakes already started to diversify in the mid- to upper-Mesozoic to occupy multiple types of Grinnellian and Eltonian niches (e.g., Albino et al., 2016; Caldwell et al., 2015; Fachini et al., 2020; Wilson et al., 2010). This was also the time when many of the snake cranial morphotypes, including those of a "generalist burrower/semi-burrower" (e.g., *Dinilysia patagonica*) and "obligate burrower" (e.g., scolecophidian *Boipeba tayassuensis* [Fachini et al., 2020]), appeared. Snakes indeed experienced a highly accelerated rate of morphological evolution during this period (Simões et al., 2020). It is, however, the "generalist burrowers" features that show reversals in multiple, more derived snake lineages. In fact, none of the oldest known snakes (viz. *Eophis*, *Parviraptor*, *Diablophis*, *Portugalophis*, etc. [Caldwell et al., 2015]) show a scolecophidian-like morphology. Therefore, it appears plausible that the original ecology of the stem snake

might be that of a "generalist" fossorial/semifossorial snake, similar to that of modern semifossorial colubroids (including aparallactines). They also possibly had a close association with both terrestrial (as suggested by Watanabe et al., 2019) and aquatic niches (indicated by the fact that mid-Mesozoic snakes were likely to be island dwellers [Caldwell et al., 2015], and by the upper-Mesozoic, snakes definitively inferred to be aquatic appeared [Caldwell & Lee, 1997; Albino et al., 2016]), like mangrove mudflat dwelling homalopsids and Asian pipe snakes (*Cylindrophis* spp.). In fact, a scenario akin to this is likely for Cretaceous *Dinilysia patagonica* (Palci et al., 2017).

4.3 | Systematics and evolution

None of the phylogenies inferred in this study recovered a monophyletic Aparallactinae. This is attributable to the lack of any defining synapomorphy of aparallactines. In contrast, Atractaspidinae have several shared apomorphies, the most notable of which pertain to their maxilla, namely, the reduction of the anterior part of the maxilla and merging of the canaliculate fang-bearing ectopterygoid process with the palatine process. The genus *Atractaspis* is highly apomorphic, in keeping with its very specialized way of living. Aparallactines' traits, on the contrary, are highly homoplasious among themselves, and snakes in general, as discussed in the preceding section. However, the c-mos phylogeny of Portillo et al. (2018) did not recover a monophyletic Aparallactinae. Interestingly, the Bayesian phylogeny from the ordered matrix contains a subclade ([*Aparallactus*, *Hypoptophis*] *Polemon*) (Figure 24a); *Aparallactus* and *Polemon* were found to be sister taxa in some molecular phylogenies (e.g., Pyron et al., 2013; Figueroa et al., 2016; these works did not have *Hypoptophis*), but not in others (e.g., Portillo et al., 2018; Zaher et al., 2019). Similarly, the c-mos topology in Portillo et al. (2018) has a subtree ((*Atractaspis*, *Homoroselaps*) (*Polemon*, *Chilorhinophis*)) which has a close analog in our unordered data tree—([(*Atractaspis*, *Homoroselaps*) *Chilorhinophis*] *Polemon*) (Figure 24b). The reason for noting all these is that there must be some phylogenetic signal (or noise) supporting the aforementioned splits that are similar between the morphological and molecular trees. Hence, it would be interesting to see the outcome of all evidence from phylogenetic analyses that have the capability to find hidden support (de Queiroz & Gatesy, 2007) for certain relationships. The phylogenetic relationships of *Hypoptophis* remain somewhat poorly resolved on account of low statistical support for its placement, though it was recovered as a sister taxon to *Aparallactus* in all the phylogenies. *Hypoptophis* was not found to be nested within any genera, and it was unique among all the examined atractaspidids in having a separate exit for the cid-nerve behind the secondary anterior opening of the vidian canal (state 1 of character statement 27). There are other differences between *Hypoptophis* and *Aparallactus*, the latter of which was the sister genus of the former in all our phylogenies, and in external morphology as well (De Witte & Laurent, 1947). Therefore, recognition of *Hypoptophis* as a monotypic genus seems justifiable.

ACKNOWLEDGMENTS

For MorphoSource scans of specimens belonging to the collection of American Museum of Natural History and California Academy of Science, the authors are grateful to Edward Stanley (University of Florida), David Kizirian (American Museum of Natural History), Lauren Scheinberg (California Academy of Science) and Eli Greenbaum (University of Texas at El Paso). For University of Michigan Museum of Zoology scan obtained from MorphoSource, the authors sincerely thank Ramon Nagesan (University of Michigan). The authors also gratefully acknowledge Digimorph.org for additional μCT scans and thank Jessica A. Maisano (University of Texas at Austin). SD and JM express gratitude to Finnish National Agency for Education for the EDUFI fellowship. (TM-19-11217) which supported part of the doctoral research of SD. SD is also gratefully acknowledges University of Helsinki LUOVA scholarship which supports SD's research work. The authors are grateful to two anonymous reviewers for highly constructive comments which helped us to improve the manuscript.

CONFLICT OF INTEREST

The authors have no conflict of interests to declare.

AUTHOR CONTRIBUTIONS

Sunandan Das: Conceptualization (equal); data curation (equal); formal analysis (lead); investigation (lead); methodology (lead); software (supporting); validation (equal); visualization (equal); writing – original draft (lead). **Jonathan Brecko:** Conceptualization (equal); data curation (lead); formal analysis (lead); investigation (equal); methodology (lead); software (lead); validation (equal); visualization (supporting); writing – original draft (equal). **Olivier S. G. Pauwels:** Conceptualization (equal); data curation (equal); investigation (equal); methodology (supporting); resources (lead); validation (equal); writing – review and editing (equal). **Juha Merilä:** Conceptualization (equal); funding acquisition (lead); investigation (equal); methodology (supporting); project administration (lead); supervision (lead); validation (equal); writing – review and editing (equal).

PEER REVIEW

The peer review history for this article is available at https://publons.com/publon/10.1002/jmor.21457.

DATA AVAILABILITY STATEMENT

The data that supports the findings of this study are available in the supplementary material of this article and MorphoSource and Digimorph repositories

ORCID

Sunandan Das https://orcid.org/0000-0002-1597-1147

REFERENCES

Albino, A., Carrillo-Briceño, J. D., & Neenan, J. M. (2016). An enigmatic aquatic snake from the Cenomanian of northern South America. *PeerJ*, *4*, e2027.

Allemand, R., Boistel, R., Daghfous, G., Blanchet, Z., Cornette, R., Bardet, N., Vincent, P., & Houssaye, A. (2017). Comparative morphology of snake (Squamata) endocasts: Evidence of phylogenetic and ecological signals. *Journal of Anatomy*, *231*(6), 849–868.

Apesteguía, S., & Zaher, H. (2006). A cretaceous terrestrial snake with robust hindlimbs and a sacrum. *Nature*, *440*(7087), 1037–1040.

Auen, E. L., & Langebartel, D. A. (1977). The cranial nerves of the colubrid snakes *Elaphe* and *Thamnophis*. *Journal of Morphology*, *154*(2), 205–222.

Bellairs, A. D. A., & Underwood, G. (1951). The origin of snakes. *Biological Reviews*, *26*(2), 193–237.

Boulenger, G. A. (1908). Descriptions of three new snakes from Africa. *Annals and Magazine of Natural History*, *8*(2), 93–94.

Bourgeois, M. (1968). Contribution à la morphologie comparée du crâne des ophidiens de l'Afrique Centrale. *Publications de l'Université Officielle du Congo à Lubumbashi*, *18*, 5–293.

Broadley, D. G. (1960). *Hypoptophis wilsoni*, a new addition to the snakes of northern Rhodesia. *Journal of the Herpetological Association of Rhodesia*, *13*(1), 5–6.

Broadley, D. G., & Cotterill, F. P. D. (2004). The reptiles of Southeast Katanga, an overlooked 'hot spot'. *African Journal of Herpetology*, *53*(1), 35–61.

Brusatte, S. L. (2012). *Dinosaur Paleobiology*. Wiley-Blackwell.

Cadle, J. E. (1994). The colubrid radiation in Africa (Serpentes: Colubridae): Phylogenetic relationships and evolutionary patterns based on immunological data. *Zoological Journal of the Linnean Society*, *110*(2), 103–140.

Caldwell, M. W. (2020). *The origin of snakes. Morphology and fossil record*. CRC Press.

Caldwell, M. W., & Lee, M. S. (1997). A snake with legs from the marine cretaceous of the Middle East. *Nature*, *386*(6626), 705–709.

Caldwell, M. W., Nydam, R. L., Palci, A., & Apesteguía, S. (2015). The oldest known snakes from the middle Jurassic-lower cretaceous provide insights on snake evolution. *Nature Communications*, *6*(1), 1–11.

Chapelle, K. E., & Choiniere, J. N. (2018). A revised cranial description of *Massospondylus carinatus* Owen (Dinosauria: Sauropodomorpha) based on computed tomographic scans and a review of cranial characters for basal Sauropodomorpha. *PeerJ*, *6*, e4224.

Chippaux, J. P., & Jackson, K. (2019). *Snakes of central and western Africa*. John Hopkins University Press.

Chretien, J., Wang-Claypool, C. Y., Glaw, F., & Scherz, M. D. (2019). The bizarre skull of *Xenotyphlops* sheds light on synapomorphies of Typhlopoidea. *Journal of Anatomy*, *234*(5), 637–655.

Cignoni, P., Callieri, Corsini, M., Dellepiane, M., Ganovelli, F., & Ranzuglia, G. (2008). *MeshLab: An open-source mesh processing tool* (pp. 129–136). Sixth Eurographics Italian Chapter Conference.

Clark, J. M., Welman, J., Gauthier, J. A., & Parrish, J. M. (1993). The laterosphenoid bone of early archosauriforms. *Journal of Vertebrate Paleontology*, *13*(1), 48–57.

Comeaux, R. S., Olori, J. C., & Bell, C. J. (2010). Cranial osteology and preliminary phylogenetic assessment of *Plectrurus aureus* Beddome, 1880 (Squamata: Serpentes: Uropeltidae). *Zoological Journal of the Linnean Society*, *160*(1), 118–138.

Conradie, W., & Pinto, P. V. (2021). A snake with an appetite for the rare: *Amblyodipsas polylepis* (Bocage, 1873) feeding on the amphisbaenid *Monopeltis luandae* Gans, 1976. *Herpetology Notes*, *14*, 205–207.

Cundall, D. (1986). Variations of the cephalic muscles in the colubrid snake genera *Entechinus*, *Opheodrys*, and *Symphimus*. *Journal of Morphology*, *187*(1), 1–21.

Cundall, D. (2020). The origin of snakes: Morphology and the fossil record. [review of the book *the origin of snakes: Morphology and the fossil record*, by M. W. Caldwell]. *Herpetological Review*, *51*(2), 364–368.

Cundall, D., & Irish, F. (2008). The snake skull. In C. Gans, A. S. Gaunt, & K. Adler (Eds.), *Biology of the Reptilia* (Vol. 20, pp. 349–692). Society for the Study of Amphibians and Reptiles.

Cundall, D., & Rossman, D. A. (1993). Cephalic anatomy of the rare Indonesian snake *Anomochilus weberi*. *Zoological Journal of the Linnean Society*, *109*(3), 235–273.

Cyriac, V. P., & Kodandaramaiah, U. (2018). Digging their own macroevolutionary grave: Fossoriality as an evolutionary dead end in snakes. *Journal of Evolutionary Biology*, *31*(4), 587–598.

da Silva, F. O., Fabre, A. C., Savriama, Y., Ollonen, J., Mahlow, K., Herrel, A., Müller, J., & di-Poï, N. (2018). The ecological origins of snakes as revealed by skull evolution. *Nature Communications*, *9*(1), 1–11.

Das, S., Campbell, P. D., Roy, S., Mukherjee, S., Pramanick, K., Biswas, A., & Raha, S. (2019). Cranial osteology and molecular phylogeny of *Argyrogena fasciolata* (Shaw, 1802) (Colubridae: Serpentes). *Vertebrate Zoology*, *69*(3), 311–325.

Das, S., & Pramanick, K. (2019). Comparative anatomy and homology of jaw adductor muscles of some south Asian colubroid snakes (Serpentes: Colubroidea). *Vertebrate Zoology*, *69*(1), 93–102.

de Queiroz, A., & Gatesy, J. (2007). The supermatrix approach to systematics. *Trends in Ecology & Evolution*, *22*(1), 34–41.

De Witte, G.-F., & Laurent, R. (1947). Révision d'un groupe de Colubridae Africains: Genres Calamelaps, Miodon, *Aparallactus* et formes affines. *Musée Royal d'Histoire Naturelle de Belgique*, *29*, 1–134.

Deufel, A. (2017). Burrowing with a kinetic snout in a snake (Elapidae: *Aspidelaps scutatus*). *Journal of Morphology*, *278*(12), 1706–1715.

Deufel, A., & Cundall, D. (2003). Feeding in *Atractaspis* (Serpentes: Atractaspididae): A study in conflicting functional constraints. *Zoology*, *106*(1), 43–61.

Douglas, R. M. (1982). A new size record and notes on feeding in captivity of *Amblyodipsas concolor* (A. Smith). *The Journal of the Herpetological Association of Africa*, *28*(1), 14–16.

Evans, S. E. (2008). The skull of lizards and tuatara. In C. Gans, A. S. Gaunt, & K. Adler (Eds.), *Biology of the Reptilia* (Vol. 20, pp. 1–347). Society for the Study of Amphibians and Reptiles.

Evans, S. E. (2016). The Lepidosaurian ear: Variations on a theme. In J. Clack, R. Fay, & A. Popper (Eds.), *Evolution of the vertebrate ear* (Vol. 59, pp. 245–284). Springer Handbook of Auditory Research, Springer.

Fachini, T. S., Onary, S., Palci, A., Lee, M. S., Bronzati, M., & Hsiou, A. S. (2020). Cretaceous blind snake from Brazil fills major gap in snake evolution. *iScience*, *23*(12), 101834.

Figueroa, A., McKelvy, A. D., Grismer, L. L., Bell, C. D., & Lailvaux, S. P. (2016). A species-level phylogeny of extant snakes with description of a new colubrid subfamily and genus. *PLoS One*, *11*(9), e0161070.

Frazzetta, T. H. (1966). Studies on the morphology and function of the skull in the Boidae (Serpentes). Part II. Morphology and function of the jaw apparatus in *Python sebae* and *Python molurus*. *Journal of Morphology*, *118*(2), 217–295.

Frazzetta, T. H. (1999). Adaptations and significance of the cranial feeding apparatus of the sunbeam snake (*Xenopeltis unicolor*): Part I. anatomy of the skull. *Journal of Morphology*, *239*(1), 27–43.

Gans, C., Dessauer, H. C., & Baic, D. (1978). Axial differences in the musculature of uropeltid snakes: The freight-train approach to burrowing. *Science*, *199*(4325), 189–192.

Garberoglio, F. F., Apesteguía, S., Simões, T. R., Palci, A., Gómez, R. O., Nydam, R. L., Larsson, H. C. E., Lee, M. S. Y., & Caldwell, M. W. (2019). New skulls and skeletons of the cretaceous legged snake *Najash*, and the evolution of the modern snake body plan. *Science Advances*, *5*(11), eaax5833.

Gauthier, J. A., Kearney, M., Maisano, J. A., Rieppel, O., & Behlke, A. D. (2012). Assembling the squamate tree of life: Perspectives from the phenotype and the fossil record. *Bulletin of the Peabody Museum of Natural History*, *53*(1), 3–308.

Greene, H. (1997). *Snakes. Evolution of mystery in nature*. California University Press.

Head, J. J., & Müller, J. (2020). Squamate reptiles from Kanapoi: Faunal evidence for hominin paleoenvironments. *Journal of Human Evolution*, *140*, 102451.

Heinicke, M. P., Titus-McQuillan, J. E., Daza, J. D., Kull, E. M., Stanley, E. L., & Bauer, A. M. (2020). Phylogeny and evolution of unique skull morphologies in dietary specialist African shovel-snouted snakes (Lamprophiidae: *Prosymna*). *Biological Journal of the Linnean Society*, *131*(1), 136–153.

Herrel, A., Lowie, A., Miralles, A., Gaucher, P., Kley, N. J., Measey, J., & Tolley, K. A. (2021). Burrowing in blindsnakes: A preliminary analysis of burrowing forces and consequences for the evolution of morphology. *The Anatomical Record*, *2021*(Special Issue), 1–11.

Hsiang, A. Y., Field, D. J., Webster, T. H., Behlke, A. D., Davis, M. B., Racicot, R. A., & Gauthier, J. A. (2015). The origin of snakes: Revealing the ecology, behavior, and evolutionary history of early snakes using genomics, phenomics, and the fossil record. *BMC Evolutionary Biology*, *15*(1), 1–22.

Kamal, A. M., & Hammouda, H. G. (1965). The development of the skull of *Psammophis sibilans*. III. The osteocranium of a late embryo. *Journal of Morphology*, *116*(2), 297–310.

Kelly, C. M., Barker, N. P., Villet, M. H., & Broadley, D. G. (2009). Phylogeny, biogeography and classification of the snake superfamily Elapoidea: A rapid radiation in the late Eocene. *Cladistics*, *25*(1), 38–63.

Kley, N. J. (2001). Prey transport mechanisms in blindsnakes and the evolution of unilateral feeding systems in snakes. *American Zoologist*, *41*(6), 1321–1337.

Kley, N. J. (2006). Morphology of the lower jaw and suspensorium in the Texas blindsnake, *Leptotyphlops dulcis* (Scolecophidia: Leptotyphlopidae). *Journal of Morphology*, *267*(4), 494–515.

Kluge, A. G. (1993). *Aspidites* and the phylogeny of pythonine snakes. *Records of the Australian Museum (Supplement)*, *19*, 1–77.

Koch, C., Martins, A., Joshi, M., Pinto, R. R., & Passos, P. (2021). Osteology of the enigmatic threadsnake species *Epictia unicolor* and *Trilepida guayaquilensis* (Serpentes, Leptotyphlopidae) with generic insights. *The Anatomical Record*, *2021*(Special Issue), 1–15.

Lewis, P. O. (2001). A likelihood approach to estimating phylogeny from discrete morphological character data. *Systematic Biology*, *50*(6), 913–925.

Lillywhite, H. B. (2014). *How snakes work: Structure, function and behavior of the World's snakes*. Oxford University Press.

Longrich, N. R., Bhullar, B. A. S., & Gauthier, J. A. (2012). A transitional snake from the late cretaceous period of North America. *Nature*, *488*(7410), 205–208.

Marais, J. (2004). *A complete guide to the snakes of southern Africa*. StruikNature.

Martill, D. M., Tischlinger, H., & Longrich, N. R. (2015). A four-legged snake from the early cretaceous of Gondwana. *Science*, *349*(6246), 416–419.

Martins, A., Koch, C., Joshi, M., Pinto, R., Machado, A., Lopes, R., & Passos, P. (2021). Evolutionary treasures hidden in the West Indies: Comparative osteology and visceral morphology reveals intricate miniaturization in the insular genera *Mitophis* hedges, Adalsteinsson, & Branch, 2009 and *Tetracheilostoma* Jan, 1861 (Leptotyphlopidae: Epictinae: Tetracheilostomina). *The Anatomical Record*, *2021*(Special Issue), 1–31.

McCartney, J. A., Stevens, N. J., & O'Connor, P. M. (2014). The earliest colubroid-dominated snake fauna from Africa: Perspectives from the late Oligocene Nsungwe formation of southwestern Tanzania. *PLoS One*, *9*(3), e90415.

McDowell, S. B. (1968). Affinities of the snakes usually called *Elaps lacteus* and *E. dorsalis*. *Zoological Journal of the Linnean Society*, *47*(313), 561–578.

McDowell, S. B. (1975). A catalogue of the snakes of New Guinea and the Solomons, with special reference to those in the Bernice P. bishop museum. Part II. Anilioidea and Pythoninae. *Journal of Herpetology*, *9*(1), 1–79.

McDowell, S. B. (1986). The architecture of the corner of the mouth of colubroid snakes. *Journal of Herpetology*, *20*(3), 353–407.

McDowell, S. B. (1987). Systematics. In R. A. Seigel, J. T. Collins, & S. S. Novak (Eds.), *Snakes: Ecology and evolutionary biology* (pp. 3–50). Macmillan.

McDowell, S. B. (2008). The skull of Serpentes. In C. Gans, A. S. Gaunt, & K. Adler (Eds.), *Biology of the Reptilia* (Vol. 21, pp. 467–620). Society for the Study of Amphibians and Reptiles.

Müller, L. (1911). Zwei neue Schlangen aus dem Katangadistrikt, Kongostaat. *Zoologischer Anzeiger*, *38*, 357–360.

Olori, J. C. (2010). Digital endocasts of the cranial cavity and osseous labyrinth of the burrowing snake *Uropeltis woodmasoni* (Alethinophidia: Uropeltidae). *Copeia*, *2010*(1), 14–26.

Olori, J. C., & Bell, C. J. (2012). Comparative skull morphology of uropeltid snakes (Alethinophidia: Uropeltidae) with special reference to disarticulated elements and variation. *PLoS One*, *7*(3), e32450.

O'Reilly, J. E., Puttick, M. N., Parry, L., Tanner, A. R., Tarver, J. E., Fleming, J., Pisani, D., & Donoghue, P. C. (2016). Bayesian methods outperform parsimony but at the expense of precision in the estimation of phylogeny from discrete morphological data. *Biology Letters*, *12*(4), 20160081.

O'Reilly, J. E., Puttick, M. N., Pisani, D., & Donoghue, P. C. (2018). Probabilistic methods surpass parsimony when assessing clade support in phylogenetic analyses of discrete morphological data. *Palaeontology*, *61*(1), 105–118.

Palci, A., & Caldwell, M. W. (2013). Primary homologies of the circumorbital bones of snakes. *Journal of Morphology*, *274*(9), 973–986.

Palci, A., & Caldwell, M. W. (2014). The upper cretaceous snake *Dinilysia patagonica* smith-Woodward, 1901, and the crista circumfenestralis of snakes. *Journal of Morphology*, *275*(10), 1187–1200.

Palci, A., Hutchinson, M. N., Caldwell, M. W., & Lee, M. S. (2017). The morphology of the inner ear of squamate reptiles and its bearing on the origin of snakes. *Royal Society Open Science*, *4*(8), 170685.

Palci, A., Hutchinson, M. N., Caldwell, M. W., Scanlon, J. D., & Lee, M. S. (2018). Palaeoecological inferences for the fossil Australian snakes *Yurlunggur* and *Wonambi* (Serpentes, Madtsoiidae). *Royal Society Open Science*, *5*(3), 172012.

Portillo, F., Branch, W. R., Conradie, W., Rödel, M. O., Penner, J., Barej, M. F., Kusamba, C., Muninga, W. M., Aristote, M. M., Bauer, A. M., Trape, J. F., Nagy, Z. T., Carlino, P., Pauwels, O. S. G., Menegon, M., Burger, M., Mazuch, T., Jackson, K., Hughes, D. F., … Greenbaum, E. (2018). Phylogeny and biogeography of the African burrowing snake subfamily Aparallactinae (Squamata: Lamprophiidae). *Molecular Phylogenetics and Evolution*, *127*, 288–303.

Portillo, F., Stanley, E. L., Branch, W. R., Conradie, W., Rödel, M. O., Penner, J., Barej, M. F., Kusamba, C., Muninga, W. M., Aristote, M. M., Bauer, A. M., Trape, J. F., Nagy, Z. T., Carlino, P., Pauwels, O. S. G., Menegon, M., Ineich, I., Burger, M., Zassi-Boulou, A. G., … Greenbaum, E. (2019). Evolutionary history of burrowing asps (Lamprophiidae: Atractaspidinae) with emphasis on fang evolution and prey selection. *PLoS One*, *14*(4), e0214889.

Pregill, G. K. (1977). Axial myology of the racer *Coluber constrictor* with emphasis on the neck region. *Transactions of the San Diego Society of Natural History*, *18*, 185–206.

Puttick, M. N., O'Reilly, J. E., Oakley, D., Tanner, A. R., Fleming, J. F., Clark, J., Holloway, L., Lozano-Fernandez, J., Parry, L. A., Tarver, J. E., Pisani, D., & Donoghue, P. C. (2017). Parsimony and maximum-likelihood phylogenetic analyses of morphology do not generally integrate uncertainty in inferring evolutionary history: A response to Brown et al. *Proceedings of the Royal Society B: Biological Sciences*, *284*(1864), 20171636.

Puttick, M. N., O'Reilly, J. E., Tanner, A. R., Fleming, J. F., Clark, J., Holloway, L., Lozano-Fernandez, J., Parry, L. A., Tarver, J. E., Pisani, D., & Donoghue, P. C. (2017). Uncertain-tree: Discriminating among competing approaches to the phylogenetic analysis of phenotype data. *Proceedings of the Royal Society B: Biological Sciences*, *284*(1846), 20162290.

Pyron, R. A., Burbrink, F. T., & Wiens, J. J. (2013). A phylogeny and revised classification of Squamata, including 4161 species of lizards and snakes. *BMC Evolutionary Biology*, *13*(1), 1–54.

Racca, L., Villa, A., Wencker, L. C., Camaiti, M., Blain, H. A., & Delfino, M. (2020). Skull osteology and osteological phylogeny of the Western whip snake *Hierophis viridiflavus* (Squamata, Colubridae). *Journal of Morphology*, *28*(7), 808–831.

Rambaut, A., Drummond, A. J., Xie, D., Baele, G., & Suchard, M. A. (2018). Posterior summarization in Bayesian phylogenetics using tracer 1.7. *Systematic Biology*, *67*(5), 901.

Rauhut, O. W., Milner, A. C., & Moore-Fay, S. (2010). Cranial osteology and phylogenetic position of the theropod dinosaur *Proceratosaurus bradleyi* (Woodward, 1910) from the middle Jurassic of England. *Zoological Journal of the Linnean Society*, *158*(1), 155–195.

Rieppel, O. (1976). The homology of the laterosphenoid bone in snakes. *Herpetologica*, *32*(4), 426–429.

Rieppel, O. (1979). The evolution of the basicranium in the Henophidia (Reptilia: Serpentes). *Zoological Journal of the Linnean Society*, *66*(4), 411–431.

Rieppel, O. (2007). The naso-frontal joint in snakes as revealed by high-resolution X-ray computed tomography of intact and complete skulls. *Zoologischer Anzeiger*, *246*(3), 177–191.

Rieppel, O., Kley, N. J., & Maisano, J. A. (2009). Morphology of the skull of the white-nosed blindsnake, *Liotyphlops albirostris* (Scolecophidia: Anomalepididae). *Journal of Morphology*, *270*(5), 536–557.

Rieppel, O., & Maisano, J. A. (2007). The skull of the rare Malaysian snake *Anomochilus leonardi* smith, based on high-resolution X-ray computed tomography. *Zoological Journal of the Linnean Society*, *149*(4), 671–685.

Rieppel, O., & Zaher, H. (2002). The skull of the Uropeltinae (Reptilia, Serpentes), with special reference to the otico-occipital region. *Bulletin of The Natural History Museum, Zoology Series*, *68*, 123–130.

Ronquist, F., Teslenko, M., Van Der Mark, P., Ayres, D. L., Darling, A., Höhna, S., Larget, B., Liu, L., Suchard, M. A., & Huelsenbeck, J. P. (2012). MrBayes 3.2: Efficient Bayesian phylogenetic inference and model choice across a large model space. *Systematic Biology*, *61*(3), 539–542.

Savitzky, A. H. (1983). Coadapted character complexes among snakes: Fossoriality, piscivory, and durophagy. *American Zoologist*, *23*(2), 397–409.

Scanlon, J. D. (2005). Cranial morphology of the Plio–Pleistocene giant madtsoiid snake *Wonambi naracoortensis*. *Acta Palaeontologica Polonica*, *50*(1), 139–180.

Scanlon, J. D. (2006). Skull of the large non-macrostomatan snake *Yurlunggur* from the Australian Oligo-Miocene. *Nature*, *439*(7078), 839–842.

Sereno, P. C. (2007). Logical basis for morphological characters in phylogenetics. *Cladistics*, *23*(6), 565–587.

Sheverdyukova, H. V., & Kovtun, M. F. (2020). Variation in the formation of crista sellaris and basisphenoid in the skull of the grass snake *Natrix natrix* embryos (Serpentes, Colubridae). *Journal of Morphology*, *281*(3), 338–347.

Shine, R., Branch, W. R., Harlow, P. S., Webb, J. K., & Shine, T. (2006). Biology of burrowing asps (Atractaspididae) from southern Africa. *Copeia*, *2006*(1), 103–115.

Shubin, N., Tabin, C., & Carroll, S. (2009). Deep homology and the origins of evolutionary novelty. *Nature*, *457*(7231), 818–823.

Simões, T. R., Vernygora, O., Caldwell, M. W., & Pierce, S. E. (2020). Megaevolutionary dynamics and the timing of evolutionary innovation in reptiles. *Nature Communications*, *11*(1), 1–14.

Spawls, S., Howell, K., Hinkel, H., & Menegon, M. (2018). *Field guide to east African reptiles*. Bloomsbury Publishing.

Strong, C. R. C., Palci, A., & Caldwell, M. W. (2020). Insights into skull evolution in fossorial snakes, as revealed by the cranial morphology of *Atractaspis irregularis* (Serpentes: Colubroidea). *Journal of Anatomy*, *238*(1), 146–172.

Swofford, D. L. (2003). *PAUP*. Phylogenetic analysis using parsimony (*and other methods). Version 4*. Sinauer Associates.

Szyndlar, Z. (1984). Fossil snakes from Poland. *Acta Zoologica Cracoviensia*, *28*, 1–156.

Tsuihiji, T. (2007). Homologies of the longissimus, iliocostalis, and hypaxial muscles in the anterior presacral region of extant Diapsida. *Journal of Morphology*, *268*(11), 986–1020.

Tsuihiji, T., Kearney, M., & Rieppel, O. (2012). Finding the neck–trunk boundary in snakes: Anteroposterior dissociation of myological characteristics in snakes and its implications for their neck and trunk body regionalization. *Journal of Morphology*, *273*(9), 992–1009.

Uetz, P., Freed, P., & Hošek, J. (2020). The reptile database, http://www.reptile-database.org

Underwood, G. (1967). *A contribution to the classification of snakes*. British Museum (Natural History).

Underwood, G., & Kochva, E. (1993). On the affinities of the burrowing asps *Atractaspis* (Serpentes: Atractaspididae). *Zoological Journal of the Linnean Society*, *107*(1), 3–64.

Vernygora, O. V., Simões, T. R., & Campbell, E. O. (2020). Evaluating the performance of probabilistic algorithms for phylogenetic analysis of big morphological datasets: A simulation study. *Systematic Biology*, *69*(6), 1088–1105.

Vonk, F. J., Admiraal, J. F., Jackson, K., Reshef, R., de Bakker, M. A., Vanderschoot, K., van den Berge, I., van Atten, M., Burgerhout, E., Beck, A., Mirtschin, P. J., Kochva, E., Witte, F., Fry, B. G., Woods, A. E., & Richardson, M. K. (2008). Evolutionary origin and development of snake fangs. *Nature*, *454*(7204), 630–633.

Wake, D. B., Wake, M. H., & Specht, C. D. (2011). Homoplasy: From detecting pattern to determining process and mechanism of evolution. *Science*, *331*(6020), 1032–1035.

Walls, G. L. (1942). *The vertebrate eye and its adaptive radiation*. Hafner Publishing Company.

Watanabe, A., Fabre, A. C., Felice, R. N., Maisano, J. A., Müller, J., Herrel, A., & Goswami, A. (2019). Ecomorphological diversification in squamates from conserved pattern of cranial integration. *Proceedings of the National Academy of Sciences*, *116*(29), 14688–14697.

Werneburg, I., & Sánchez-Villagra, M. R. (2015). Skeletal heterochrony is associated with the anatomical specializations of snakes among squamate reptiles. *Evolution*, *69*(1), 254–263.

Wilson, J. A., Mohabey, D. M., Peters, S. E., & Head, J. J. (2010). Predation upon hatchling dinosaurs by a new snake from the late cretaceous of India. *PLoS Biology*, *8*(3), e1000322.

Wright, A. M., & Hillis, D. M. (2014). Bayesian analysis using a simple likelihood model outperforms parsimony for estimation of phylogeny from discrete morphological data. *PLoS One*, *9*(10), e109210.

Yi, H., & Norell, M. A. (2015). The burrowing origin of modern snakes. *Science Advances*, *1*(10), e1500743.

Zaher, H., Murphy, R. W., Arredondo, J. C., Graboski, R., Machado-Filho, P. R., Mahlow, K., Montingelli, G. G., Quadros, A. B., Orlov, N. L., Wilkinson, M., Zhang, Y. P., & Grazziotin, F. G. (2019). Large-scale molecular phylogeny, morphology, divergence-time estimation, and the fossil record of advanced caenophidian snakes (Squamata: Serpentes). *PLoS One*, *14*(5), e0216148.

Zaher, H., & Scanferla, C. A. (2012). The skull of the upper cretaceous snake *Dinilysia patagonica* smith-Woodward, 1901, and its phylogenetic position revisited. *Zoological Journal of the Linnean Society*, *164*(1), 194–238.

Zheng, Y., & Wiens, J. J. (2016). Combining phylogenomic and supermatrix approaches, and a time-calibrated phylogeny for squamate reptiles (lizards and snakes) based on 52 genes and 4162 species. *Molecular Phylogenetics and Evolution*, *94*, 537–547.

SUPPORTING INFORMATION

Additional supporting information may be found in the online version of the article at the publisher's website.

How to cite this article: Das, S., Brecko, J., Pauwels, O. S. G., & Merilä, J. (2022). Cranial osteology of *Hypoptophis* (Aparallactinae: Atractaspididae: Caenophidia), with a discussion on the evolution of its fossorial adaptations. *Journal of Morphology*, *283*(4), 510–538. https://doi.org/10.1002/jmor.21457